Maternal age affects equine Day 8 embryo gene expression both in trophoblast and inner cell mass

E. Derisoud, L. Jouneau, C. Dubois, C. Archilla, Y. Jaszczyszyn, R. Legendre, N. Daniel, N. Peynot, Michèle Dahirel, J. Auclair-Ronzaud, et al.

▶ **To cite this version:**

E. Derisoud, L. Jouneau, C. Dubois, C. Archilla, Y. Jaszczyszyn, et al.. Maternal age affects equine Day 8 embryo gene expression both in trophoblast and inner cell mass. 2021. hal-03695686v1

HAL Id: hal-03695686

https://hal.science/hal-03695686v1

Preprint submitted on 17 Nov 2021 (v1), last revised 15 Jun 2022 (v2)

HAL is a multi-disciplinary open access archive for the deposit and dissemination of scientific research documents, whether they are published or not. The documents may come from teaching and research institutions in France or abroad, or from public or private research centers.

L'archive ouverte pluridisciplinaire **HAL**, est destinée au dépôt et à la diffusion de documents scientifiques de niveau recherche, publiés ou non, émanant des établissements d'enseignement et de recherche français ou étrangers, des laboratoires publics ou privés.

Distributed under a Creative Commons Attribution - NonCommercial - NoDerivatives 4.0 International License

bioRxiv preprint doi: https://doi.org/10.1101/2021.04.07.438786; this version posted April 9, 2021. The copyright holder for this preprint (which was not certified by peer review) is the author/funder, who has granted bioRxiv a license to display the preprint in perpetuity. It is made available under aCC-BY-NC-ND 4.0 International license.

Maternal age affects equine Day 8 embryo gene expression both in trophoblast and inner cell mass

E. Derisoud[1,2], L. Jouneau[1,2], C. Dubois[3], C. Archilla[1,2], Y. Jaszczyszyn[4], R. Legendre[5], N. Daniel[1,2], N. Peynot[1,2], M. Dahirel[1,2], J. Auclair-Ronzaud[3], L. Wimel[3], V. Duranthon[1,2], P. Chavatte-Palmer[1,2]

[1] Université Paris-Saclay, UVSQ, INRAE, BREED, 78350, Jouy-en-Josas, France

[2] Ecole Nationale Vétérinaire d'Alfort, BREED, 94700, Maisons-Alfort, France

[3] IFCE, Plateau technique de la Valade, Chamberet, France

[4] Institute for Integrative Biology of the Cell (I2BC), UMR 9198 CNRS, CEA, Paris-Sud University F-91198, Gif-sur-Yvette, France

[5] Institut Pasteur—Bioinformatics and Biostatistics Hub—Department of Computational Biology, USR 3756 IP CNRS, Paris, France

Corresponding authors:

Emilie Derisoud

emilie.derisoud@gmail.com

Pascale Chavatte-Palmer

pascale.chavatte-palmer@inrae.fr

Declarations

bioRxiv preprint doi: https://doi.org/10.1101/2021.04.07.438786; this version posted April 9, 2021. The copyright holder for this preprint (which was not certified by peer review) is the author/funder, who has granted bioRxiv a license to display the preprint in perpetuity. It is made available under aCC-BY-NC-ND 4.0 International license.

Ethics approval and consent to participate

The experiment was performed at the experimental farm of IFCE (research agreement C1903602 valid until March 22, 2023). The protocol was approved by the local animal care and use committee ("Comité des Utilisateurs de la Station Expérimentale de Chamberet") and by the regional ethical committee ("Comité Régional d'Ethique pour l'Expérimentation Animale du Limousin", approved under N° C2EA - 33 in the National Registry of French Ethical Committees for animal experimentation) under protocol number APAFIS#14963-2018050316037888 v2. All experiments were performed in accordance with the European Union Directive 2010/63EU.

Consent for publication

Not applicable

Availability of data and materials

The RNA sequençing data supporting the conclusions of this article are available in the GEO repository, [accession: GSE162893; https://www.ncbi.nlm.nih.gov/geo/query/acc.cgi?acc=GSE162893].

Competing interests

The authors declare that they have no competing interests.

Funding

This work was supported by the "Institut Français du Cheval et de l'Equitation" (grant numbers CS_2018_23, 2018). The National Research Institute for Agriculture, Food and Environment (INRAE) department Animal Physiology and Breeding Systems also supported this research.

bioRxiv preprint doi: https://doi.org/10.1101/2021.04.07.438786; this version posted April 9, 2021. The copyright holder for this preprint (which was not certified by peer review) is the author/funder, who has granted bioRxiv a license to display the preprint in perpetuity. It is made available under aCC-BY-NC-ND 4.0 International license.

Author contribution statement

PCP obtained the funding. PCP and VD conceived the project. LW, PCP, and VD supervised the study. ED, CD, CA, ND, NP, LW, VD and PCP adapted the methodology for the project. ED, CD, CA, YJ, JAR, and LW performed the experiments. CD, CA, ND, NP, MD and LW provided the resources. ED, LJ, YJ and RL performed data curation. ED and LJ analysed the data. ED wrote the original draft. All authors read, revised, and approved the submitted manuscript.

Acknowledgments

The authors are grateful to the staff of the Institut Français du Cheval et de l'Equitation (IFCE) experimental farm (Domaine de la Valade, Chamberet, France) for care and management of animals. We acknowledge the High-throughput sequencing facility of I2BC for its sequencing and bioinformatics expertise. The bioinformatics analyses were performed thanks to Core Cluster of the Institut Français de Bioinformatique (IFB) (ANR-11-INBS-0013). Many thanks to Matthias Zytnicki and Christophe Klopp for their advice on RNA-seq de novo analysis. Many thanks to Pablo Ross who kindly provided the coordinates for the XIST gene. The authors thank Shavahn Loux for her information on PLAC8A. The authors are grateful to Alice Jouneau and Sophie Calderari who kindly revised this article.

Abstract

Background: Increased embryo loss as mares become older is a major consideration for breeders as older animals are currently used for reproduction in the equine industry. Lower embryo quality has been pointed out as partly responsible for this reduced fertility. Here, the effect of mare's age on blastocysts' gene expression was explored. Day 8 post ovulation embryos were collected by uterine flushing from multiparous young (YM, 6-year-old, N = 5) and older (OM, > 10-year-old, N = 6) non-

bioRxiv preprint doi: https://doi.org/10.1101/2021.04.07.438786; this version posted April 9, 2021. The copyright holder for this preprint (which was not certified by peer review) is the author/funder, who has granted bioRxiv a license to display the preprint in perpetuity. It is made available under aCC-BY-NC-ND 4.0 International license.

nursing Saddlebred mares, inseminated with the semen of one stallion. Pure (TE_part) or inner cell mass enriched (ICMandTE) trophoblast were obtained by embryo bisection and paired end, non-oriented RNA sequencing (Illumina, NextSeq500) was performed on each hemi-embryo. To discriminate gene expression in the ICM from that in the TE, deconvolution (DeMixT R package) was used on the ICMandTE dataset. Differential expression was analyzed (DESeq2) with embryo sex and diameter as cofactors using a false discovery rate < 0.05 cutoff. Functional annotation and classification of differentially expressed genes and gene set enrichment analysis were also performed.

Results: Maternal aging did not affect embryo recovery rate, embryo diameter nor total RNA quantity but modified gene expression in equine D8 embryos. The expression of genes in the ICM seemed to be more altered by maternal aging than in the TE. In both compartments, the expression of genes involved in mitochondrial function, translation and transcription due to chromatin modification were disturbed by maternal age. Mitosis, signaling and adhesion pathways and embryo development were particularly decreased in the ICM hemi-embryos from old mares. Finally, in TE, ion movement related genes were affected.

Conclusions: This is the first study showing an effect of maternal age on gene expression in the equine blastocyst at Day 8 post ovulation. Maternal age, even for mares as young as 10 years old, disturbs mitosis, translation and transcription, cell signaling and adhesion as well as mitochondrial function and cell commitment of horse embryos. These perturbations may affect further embryo development and contribute to decreased fertility due to aging.

Keywords

horse; aging; blastocyst; methylation; mitochondria; mitosis; cell commitment

bioRxiv preprint doi: https://doi.org/10.1101/2021.04.07.438786; this version posted April 9, 2021. The copyright holder for this preprint (which was not certified by peer review) is the author/funder, who has granted bioRxiv a license to display the preprint in perpetuity. It is made available under aCC-BY-NC-ND 4.0 International license.

Background

Unlike other farm animals, the main purpose for the use of horses is athletic performance and leisure. In many cases, mares produce foals regularly to remain profitable after their sport career so that their reproductive career may last until advanced age, even though mares' fertility declines with age [1]. Indeed, in Thoroughbreds, pregnancy rates per estrous at Day 42 post-ovulation were shown to be reduced from 63.0% in young mares to 58.5% in mares older than 9 , and to reach 43.8% in mares older than 18 [2]. One study on 535,746 fertility records in mixed breeds in France showed that if a 10% of fertility decline is chosen as cutoff value for culling breeding mares, then mares older than 8 should not be bred [3].

Embryo collections and transfers at various developmental stages have been performed to determine at what stage embryos are affected and whether embryo or uterine quality is responsible for the fertility decline. Uterine blood flow during the luteal phase (Day 12-20 post ovulation) was reduced in mares >15 years old compared to mares <6 years old [4]. Moreover, at 2 days post ovulation, using oviductal flushes, the fertilization rate was similar between young and fertile mares *vs* old and subfertile mares (respectively, 10/14 *vs* 11/14 embryos recovered per group on Day 2). In contrast, in the same study, using the same mares on another estrus period, a significantly higher pregnancy rate at 14 days post ovulation was observed in young and fertile mares (respectively, 12/15 *vs* 3/15 pregnant mares on Day 14 by ultrasonography) [5]. Moreover, in practice, embryo loss is generally higher between the first (14 - 22 days) and the second (42 - 45 days) pregnancy check in old compared to young mares [2,6,7]. Using a ROC analysis based on 11 years of data from nursing Thoroughbred mares in Brazil, the cutoff value for embryo mortality to reach above average values was calculated to be 10 years of age [7]. In addition, Day 4 embryos collected from old and subfertile mares and directly transferred in synchronized young and fertile mares, were shown to result in lower pregnancy rates at 14 days post ovulation compared to embryos from young and fertile mares transferred in the same recipient group. This was true even when only good quality embryos were considered [8]. Thus,

bioRxiv preprint doi: https://doi.org/10.1101/2021.04.07.438786; this version posted April 9, 2021. The copyright holder for this preprint (which was not certified by peer review) is the author/funder, who has granted bioRxiv a license to display the preprint in perpetuity. It is made available under aCC-BY-NC-ND 4.0 International license.

120 embryo loss seems to be the principal cause of the fertility decline in old mares, even if uterine
121 degeneration is also observed in old mares.
122 In terms of embryo morphology, the effect of maternal age is not so clear, as studies demonstrated a
123 reduction of embryo size in old mares while others did not detect any effect of maternal aging on
124 embryo size. In these studies, however, the developmental stage was not uniform, which might lead
125 to these disparities [5,8–15]. For stages of development that take place in the oviduct, *i.e.*, from
126 fertilization to the late morula stage, one study on embryos collected *in vivo* on Day 1.5 post ovulation
127 showed that embryos have the same number of cells but a poorer morphology grade (uniformity of
128 cell size and texture, imperfections and abnormalities) when mares are older than 15 [11]. In addition,
129 when mares were older than 20 years, Day 3 post ovulation embryos were shown to combine a poorer
130 morphology grade with reduced cell number [11]. In contrast, in other studies, no difference according
131 to maternal age was observed in terms of diameter or number, size, texture of blastomeres of embryos
132 collected in oviducts on Days 2 and 4 post ovulation [5,8]. For later stages, the size of embryos collected
133 on Days 7 to 10 post-ovulation, in commercial embryo transfer programs in Italy, was reduced in mares
134 older than 16 years of age, without any morphological grade alteration [10]. In contrast, smaller
135 embryos, with a higher incidence of morphological abnormalities, were collected when donors were
136 subfertile and/or 18 years old mares compared to 4 years old nulliparous mares [12]. In embryos
137 produced by intracytoplasmic sperm injection (ICSI), maternal age did not affect blastomere size, nor
138 the presence of ooplasm fragments, nor membrane extrudates through zona pellucida at 24h post-
139 ICSI [9]. Embryo cell number at the time of transfer (between 6 and 9 days post-ICSI), however, was
140 higher in embryos collected from mares older than 20 [8].
141 In terms of functional potential, a reduced quantity of mitochondrial DNA, but not genomic DNA, has
142 been reported in Day 7 embryos from mares older than 16 [16]. These data suggest that old mares'
143 blastocysts have the same number of cells than those of younger mares, but with less mitochondria
144 [16], which could be a cause or an effect of compromised embryo development in old mares.
145 Moreover, embryos from mares older than 15 seem to be less mobile before implantation than those

bioRxiv preprint doi: https://doi.org/10.1101/2021.04.07.438786; this version posted April 9, 2021. The copyright holder for this preprint (which was not certified by peer review) is the author/funder, who has granted bioRxiv a license to display the preprint in perpetuity. It is made available under aCC-BY-NC-ND 4.0 International license.

146 from mares aged 5-6 [14]. This could indicate impaired embryo development, alteration of uterine
147 contractions or both.
148 Altogether, these data indicate that the quality of embryos from older mares is reduced. Subsequently,
149 dam age could also affect placental and fetal intrauterine and offspring post-natal growth and long-
150 term health, in the context of the Developmental Origins of Health and Diseases (DOHaD) [17]. To our
151 knowledge, the role of the embryo *per se*, however, has not yet been explored. Moreover, age and
152 parity are generally positively correlated and their respective impact have not been determined yet.
153 The aim of this study was to determine the effect of maternal age in the mare on embryo gene
154 expression at the blastocyst stage. Young (<10 years) and older (>10 years) multiparous mares were
155 inseminated with the same stallion. Blastocysts were collected and bisected to separate the pure
156 trophoblast (TE_part) from the inner cell mass enriched hemi-embryo (ICMandTE). Gene expression
157 was analyzed by RNA-seq in each compartment. Deconvolution was used to isolate gene expression of
158 inner cell mass from trophoblast cells in ICMandTE part. Results shows that maternal age alters gene
159 expression of both equine Day 8 trophoblast and inner cell mass.

160

161 ## Materials and methods

162 *Ethics*

163 The experiment was performed at the experimental farm of IFCE (research agreement C1903602 valid
164 until March 22, 2023). The protocol was approved by the local animal care and use committee ("Comité
165 des Utilisateurs de la Station Expérimentale de Chamberet") and by the regional ethical committee
166 ("Comité Régional d'Ethique pour l'Expérimentation Animale du Limousin", approved under N° C2EA -
167 33 in the National Registry of French Ethical Committees for animal experimentation) under protocol
168 number APAFIS#14963-2018050316037888 v2. All experiments were performed in accordance with
169 the European Union Directive 2010/63EU.

bioRxiv preprint doi: https://doi.org/10.1101/2021.04.07.438786; this version posted April 9, 2021. The copyright holder for this preprint (which was not certified by peer review) is the author/funder, who has granted bioRxiv a license to display the preprint in perpetuity. It is made available under aCC-BY-NC-ND 4.0 International license.

Embryo collection

Thirty-one multiparous Saddlebred mares (French Anglo-Arabian and Selle Français breeds) were included in this study. Multiparous mares were defined as dams that had already foaled at least once. Mares were bred and raised in the "Institut Français du Cheval et de l'Equitation" experimental farm (Chamberet, France, 45° 34'55.17"N, 1°43'16.29"E, 442m). During the experimental protocol, mares were managed in herds in natural pastures 24h/day with free access to water. The experiments took place from April 1st to May 23rd, 2019. All mares remained healthy during this period.

Mares were allocated to 2 groups according to their age: young mares (YM, < 10 years, n = 11) and older mares (OM, ≥ 10 years, n = 20). The age threshold was defined in accordance with the literature [3,7]. Before experimentation, mare's withers' height was measured. During the experimentation, mares were weighted and mares' body condition score (BCS, scale 1 to 5) was determined by one trained operator [18]. Mares' characteristics are detailed in Table 1.

Table 1: Mares' characteristics at embryo collection time.

Characteristics	**Young mares (YM)** ***(n=11)***	**Old mares (OM)** ***(n=20)***
Breed	AA n = 1; SF n =9; SB n=1	AA n = 13; SF n = 7
Age *(in years)*	6.00 ± 0.00	11.95 ± 2.11
Parity *(number of foalings)*	1.00 ± 0.00	3.20 ± 1.15
Weight *(in kg)*	536.62 ± 44.12	589.35 ± 57.34
BCS *(scale 1-5)*	2.16 ± 0.28	2.61 ± 0.32
Withers' height *(in cm)*	157.95 ± 3.74	161.21 ± 4.23

All mares were multiparous.

AA: Anglo Arab or Anglo-Arabian type; SF: Selle Français; SB: Saddlebred; BCS: Body Condition Score.

Age, parity, weight, BCS and height are presented as mean ±SD

bioRxiv preprint doi: https://doi.org/10.1101/2021.04.07.438786; this version posted April 9, 2021. The copyright holder for this preprint (which was not certified by peer review) is the author/funder, who has granted bioRxiv a license to display the preprint in perpetuity. It is made available under aCC-BY-NC-ND 4.0 International license.

189 The mares' estrous period was monitored routinely by ultrasound with a 5MHz trans-rectal transducer.
190 During estrus, ovulation was induced with a single injection of human chorionic gonadotropin (i.v.; 750
191 - 1500IU; Chorulon® 5000; MSD Santé animale, France) as soon as one ovarian follicle > 35mm in
192 diameter was observed, together with marked uterine edema. Ovulation usually takes place within
193 48h, with > 80% occurring 25 to 48h after injection [19,20]. At the same time, mares were inseminated
194 once with fresh or refrigerated semen containing at least 1 billion motile spermatozoa from a single
195 fertile stallion. Ovulation was confirmed within the next 48 hours by ultrasonography.

196 Embryos were collected by non-surgical uterine lavage using prewarmed (37°C) lactated Ringer's
197 solution (B.Braun, France) and EZ-Way Filter (IMV Technologies, France) 10 days after insemination,
198 i.e. approximately 8 days post ovulation. Just after embryo collection, mares were treated with
199 luprotiol an analogue of prostaglandin F2α (i.m; 7.5 mg; Prosolvin, Virbac, France).

200

201 *Embryo bisection and RNA extraction*

202 Collected embryos were immediately observed using a binocular magnifying glass and photographed
203 with a size standard. Embryo diameter was subsequently determined on photographs using ImageJ®
204 software (version 1.52a; National Institutes of Health, Bethesda, MD, USA). Embryos were washed 4
205 times in commercially available Embryo holding medium (IMV Technologies, France) at 34°C and then
206 bisected with a microscalpel under binocular magnifying glass to separate trophoblast part, at this
207 stage composed of trophectoderm and endoderm (TE_part) from inner cell mass (composed of
208 epiblast cells) enriched hemi-embryos (ICMandTE) (Figure 1). Each hemi-embryo was transferred to an
209 Eppendorf DNA LoBind tube (Eppendorf, Montesson, France) with extraction buffer (PicoPure RNA
210 isolation kit, Applied Biosystems, France) and incubated for 30 min at 42°C prior to storage at - 80°C.

211 RNA was extracted from each hemi-embryo following the manufacturer's instructions using PicoPure
212 RNA isolation kit (PicoPure RNA isolation kit, Applied Biosystems, France), which included a DNAse

bioRxiv preprint doi: https://doi.org/10.1101/2021.04.07.438786; this version posted April 9, 2021. The copyright holder for this preprint (which was not certified by peer review) is the author/funder, who has granted bioRxiv a license to display the preprint in perpetuity. It is made available under aCC-BY-NC-ND 4.0 International license.

213 treatment. RNA quality and quantity were assessed with the 2100 Bioanalyzer system using RNA 6000
214 Pico or nano kit (Agilent Technologies, France) according to the manufacturer's instructions (Additional
215 file 1).

216

217 *RNA sequencing*

218 Five nanograms of total RNA were mixed (Additional file 1) with ERCC spike-in mix (Thermofisher
219 Scientific, France) according to manufacturer recommendations. Messenger RNAs were reverse
220 transcribed and amplified using the SMART-Seq V4 ultra low input RNA kit (Clontech, France) according
221 to the manufacturer recommendations. Nine PCR cycles were performed for each hemi-embryo. cDNA
222 quality was assessed on an Agilent Bioanalyzer 2100, using an Agilent High Sensitivity DNA Kit (Agilent
223 Technologies, France). Libraries were prepared from 0.15 ng cDNA using the Nextera XT Illumina library
224 preparation kit (Illumina, France). Libraries were pooled in equimolar proportions and sequenced
225 (Paired end 50-34 pb) on NextSeq500 instrument, using a NextSeq 500 High Output 75 cycles kit
226 (Illumina, France) (Additional file 1). Demultiplexing was performed with bcl2fastq2 version 2.2.18.12
227 (Illumina, France) and adapters were trimmed with Cutadapt version 1.15 [21]. Only reads longer than
228 10pb were kept.

229

230 *Embryo sexing*

231 Embryo sex was determined for each embryo in order to take in consideration embryo sex in the
232 statistical analysis as sexual dimorphism was observed in blastocysts in other species [22].

233 The expression of *X Inactive Specific Transcript* (*XIST*) was analyzed. *XIST* is a long noncoding RNA from
234 chromosome X responsible for X inactivation when two X chromosomes are present, meaning that
235 only female embryos express *XIST*. *XIST* was shown to be expressed in equine female blastocysts on
236 Day 8 post ovulation [23,24]. *XIST* is not annotated in the available equine Ensembl 3.0.99 or NCBI

bioRxiv preprint doi: https://doi.org/10.1101/2021.04.07.438786; this version posted April 9, 2021. The copyright holder for this preprint (which was not certified by peer review) is the author/funder, who has granted bioRxiv a license to display the preprint in perpetuity. It is made available under aCC-BY-NC-ND 4.0 International license.

annotation. Thus, a *de novo* transcript assembly was made using StringTie version 2.1.2 [25] following manufacturer instructions to identify *XIST* in equine embryo samples (Additional file 1). The genome annotation file output was aligned on Ensembl 99 EquCab3.0 assembly using IGV version 2.7.2 [26]. As *XIST* position and length on X chromosome has been previously determined (Pablo Ross, personal communication, [23]) and as *XIST* is annotated in humans, the most similar contig was selected. The obtained *XIST* sequence was 22,600 bp long and composed of 8 exons and 7 introns. *XIST* sequence was added to FASTA files from Ensembl 99 EquCab3.0 assembly and to the genome annotation file from Ensembl 99 EquCab3.0 assembly as a unique fictitious chromosome with one gene composed of one transcript.

XIST expression differed between individuals but was relatively close in quantification between related hemi-embryos. Therefore, seven embryos were determined as females (4 in the YM group and 3 in the OM group) while 4 were considered as males (1 in the YM group, and 3 in the OM group).

RNA mapping and counting

Alignment was performed using STAR version 2.6 [27] (2-pass mapping with the genome annotation file using the following parameters: --alignSoftClipAtReferenceEnds No --alignEndsType EndToEnd --alignIntronMax 86545 --alignMatesGapMax 86545) on previously modified Ensembl 99 EquCab3.0 assembly and annotation. Genes were then counted with featureCounts [28] from Subreads package version 1.6.1 (parameters: -p -B -C -M) (Additional file 1).

Data analysis

All statistical analyses were performed by comparing OM to YM (set as reference group) using R version 4.0.2 [29] on Rstudio software version 1.3.1056 [30].

bioRxiv preprint doi: https://doi.org/10.1101/2021.04.07.438786; this version posted April 9, 2021. The copyright holder for this preprint (which was not certified by peer review) is the author/funder, who has granted bioRxiv a license to display the preprint in perpetuity. It is made available under aCC-BY-NC-ND 4.0 International license.

261 ***Embryo recovery rate, embryo diameter and total RNA content analysis***

262 Embryo recovery rates (ERR) were calculated as number of attempts with at least one embryo
263 collected/total number of attempts. They were analyzed using the Exact Fisher test to determine if age
264 influences embryo recovery rate.

265 For total RNA content analysis, as embryos were bisected without strict equality for each hemi-
266 embryo, a separate analysis of ICMandTE and TE_part RNA quantities would not be meaningful. Thus,
267 ICMandTE and TE_part RNA quantities were initially summed up and analyzed using a mixed linear
268 model from nlme package version 3.1-148 [31], followed by 1000 permutations using PermTest
269 function from pgirmess package version 1.6.9 [32]. Maternal age and embryo sex were considered as
270 random effects.

271 Embryo diameter was analyzed with a fixed effects linear model of nlme package version 3.1-148 [31]
272 including maternal age and embryo sex, followed by 1000 permutations using PermTest function from
273 pgirmess package version 1.6.9 [32]. Variables were kept in models when statistically significant
274 differences were observed. Differences were considered as significant for $p < 0.05$.

275 Moreover, the relation between embryo size and total RNA quantity/embryo was studied and
276 represented using the nonlinear regression analysis (fitness to exponential growth equation) in
277 GraphPad Prism software 8.0.1 for Windows (Graphpad Software, San Diego, California USA,
278 www.graphpad.com).

279

280 ***Deconvolution of gene expression in ICMandTE using DeMixT***

281 A filter on counts obtained with featureCounts was applied: all genes with more than 3 non null count
282 values in at least one group (OM or YM) per hemi-embryo (ICMandTE or TE_part) were conserved. The
283 ICMandTE hemi-embryo was composed of both trophoblast and inner cell mass in unknown relative
284 proportions. In order to estimate the relative gene expression of both cell types, the DeMixT R package

bioRxiv preprint doi: https://doi.org/10.1101/2021.04.07.438786; this version posted April 9, 2021. The copyright holder for this preprint (which was not certified by peer review) is the author/funder, who has granted bioRxiv a license to display the preprint in perpetuity. It is made available under aCC-BY-NC-ND 4.0 International license.

version 1.4.0 was used [33,34]. Starting from a dataset obtained from one cell type, DeMixT estimates the proportion of cells in the mixed samples and performs a deconvolution algorithm on gene expression. TE_part (reference cells) and ICMandTE (mixed cells type) datasets were thus analyzed using the following options: niter=10; nbin=50; if.filter=TRUE; ngene.selected.for.pi=1500; ngene. Profile.selected=1500; nspikein=0. Since the deconvolution algorithm cannot be performed in the presence of null values, the value "1" was added to all count values in ICMandTE and TE_part data tables. Moreover, variance in reference cell dataset (TE_part) must not be null and gene with null variance had been removed prior to the deconvolution. Output datasets were DeMixT_ICM_cells and DeMixT_TE_cells, corresponding to the deconvoluted gene expression in ICM cells and TE cells of ICMandTE, respectively.

Quality checks for deconvolution

At the end of deconvolution, a quality check is automatically performed by the analysis: for every gene, if the difference of average of deconvoluted expression of reference cells in mixed samples (here, gene expression of TE cells in ICMandTE dataset, *i.e.,* DeMixT_TE_cells) and average of expression of reference cells (here, gene expression of TE cells in TE_part) is > 4, then, the deconvolution for concerned genes is not reliable. Therefore, genes in this case are filtered out.

Moreover, outputs of DeMixT_ICM_cells *vs* DeMixT_TE_cells, DeMixT_ICM_cells *vs* TE_part and ICMandTE *vs* TE_part were compared with Deseq2 version 1.28.1 [35] to confirm that the deconvolution was effective at separating gene expression. Moreover, several genes proper to ICM and TE cells in equine embryos were identified using literature search [23]. Their raw and deconvoluted expressions were analyzed to check the reliability of deconvolution. Results of these analyses were represented through manually drawn Venn diagrams as well as principal component analysis graphics of individuals, using ggplot2 version 3.3.3 [36] and factoextra version 1.0.7 [37].

bioRxiv preprint doi: https://doi.org/10.1101/2021.04.07.438786; this version posted April 9, 2021. The copyright holder for this preprint (which was not certified by peer review) is the author/funder, who has granted bioRxiv a license to display the preprint in perpetuity. It is made available under aCC-BY-NC-ND 4.0 International license.

310 ***Maternal age comparison for gene expression***

311 For the comparison of maternal age, ICMandTE, DeMixT_ICM_cells and TE_part datasets were used
312 and a filter was applied on datasets: all genes with an average expression equal or above 10 counts in
313 at least one group (OM or YM) per hemi-embryo (ICM or TE) were conserved. Differential analyses
314 were performed with Deseq2 version 1.28.1 [35] with YM group as reference, without independent
315 filtering and taking into account embryo diameter and sex in the model. Genes were considered
316 differentially expressed (DEG) for FDR < 0.05 after Benjamini-Hochberg correction (also known as false
317 discovery rate, FDR).

318 Equine Ensembl IDs were converted into Human Ensembl IDs and Entrez Gene names using gorth
319 function in gprofiler2 package version 0.1.9 [38]. Genes without Entrez Gene names using gprofiler2
320 were manually converted when Entrez Gene names were available, using Ensembl web search function
321 [39].

322 Moreover, DEG were analyzed for classification, over- and under- representation (FDR < 0.05) using
323 Fisher's exact test corrected with FDR and using the database Gene Ontology (GO) Biological Process
324 complete on PANTHER version 16.0 web-based software [40]. Only the most specific subclass
325 pathways, provided by PANTHER's automated hierarchy sorting, were conserved and represented.

326

327 ***Gene set enrichment analyses (GSEA)***

328 The count values were log transformed using RLOG function of DESeq2 version 1.28.1. Gene set
329 enrichment analyses (GSEA) were performed on expressed genes using GSEA software version 4.0.3
330 (Broad Institute, Inc., Massachusetts Institute of Technology, and Regents of the University of
331 California) [41,42] to identify biological gene sets disturbed by age. GSEA was performed using the
332 following parameters: 1000 gene set permutations, weighted enrichment analysis, gene set size
333 between 15 and 500, signal-to-noise metrics. Molecular Signatures Database [43] version 7.1 (C2:

bioRxiv preprint doi: https://doi.org/10.1101/2021.04.07.438786; this version posted April 9, 2021. The copyright holder for this preprint (which was not certified by peer review) is the author/funder, who has granted bioRxiv a license to display the preprint in perpetuity. It is made available under aCC-BY-NC-ND 4.0 International license.

KEGG: Kyoto Encyclopedia of Genes and Genomes, C5: BP: GO biological process) were used to identify most perturbed pathways. Pathways were considered significantly enriched for FDR < 0.05. When normalized enrichment score (NES) was positive, the gene set was enriched in the OM group while when NES was negative, the gene set was enriched in the YM group.

Enriched terms from GO BP and KEGG database were represented using SUMER analysis from SUMER R package version 1.1.5 and using FDR q-values [44]. First, SUMER analysis reduces redundancy using weighted set cover algorithm and then clusters the results using affinity propagation algorithm. The weighted set cover algorithm performs a selection of the fewest number of gene sets that include all genes associated with the enriched sets, giving priority for the most significant terms. Then, the affinity propagation algorithm groups similar gene sets and identifies one representative gene set. This algorithm will repeat this clustering to obtain the most representative gene sets. Results were represented with graph modified using Cytoscape version 3.8.2 [45]. Gene sets were represented by nodes and the gene set size was represented by the size of the node. Node shape represented the gene set database (GO BP or KEGG). Blue nodes represented gene sets enriched in YM (NES < 0) while red nodes represented gene sets enriched in OM (NES > 0). Edge width represents the level of connection between representative gene sets (thinner edges represent the first clustering while thicker edges represent the second clustering of the affinity propagation algorithm)

Results

Embryo rates, diameter, total RNA content and quality

Altogether, 36 uterine flushings were performed (12 in YM and 24 in OM, 5 mares being flushed twice). No twin embryos were obtained. Embryo recovery rate was 42% and 25% in YM and OM, respectively and did not differ between groups (p = 0.45). All embryos were expanded blastocysts grade I or II according to the embryo classification of McKinnon and Squires [46].

bioRxiv preprint doi: https://doi.org/10.1101/2021.04.07.438786; this version posted April 9, 2021. The copyright holder for this preprint (which was not certified by peer review) is the author/funder, who has granted bioRxiv a license to display the preprint in perpetuity. It is made available under aCC-BY-NC-ND 4.0 International license.

Embryo diameter ranged from 409 µm to 2643 µm, with no effect of group on embryo diameter (p = 0.97). RNA yield per embryo ranged from 16 ng to 2915.5 ng and was not related to mares' age (p = 0.92). There is a clear exponential relation between RNA yield/embryo and embryo size (Figure 2). The median RNA Integrity Number (RIN) was 9.8 (8.7 - 10 range). Between 29.4 and 69.5 million reads per sample were obtained after trimming. On average, 83.61% of reads were mapped on the modified EquCab 3.0 using STAR and 66.66% of reads were assigned to genes by featureCounts.

Deconvolution of gene expression to discriminate ICM and TE gene expression in ICMandTE hemi-embryos

After keeping genes with less than 3 non null count values in at least one group (OM or YM) per hemi-embryo (ICMandTE or TE_part), 16,741 genes were conserved for deconvolution. In addition, twenty-seven genes were removed because their variance was null in the TE_part. However, for these genes, the mean counting in ICMandTE samples was above 10 counts, excepted for one which had a mean expression of 34 counts. On the other hand, this gene was only expressed in 5 ICMandTE over the 10 counts threshold.

During the analysis, 3 additional genes were excluded because the deconvolution quality for these genes was not sufficient. Therefore, at the end of deconvolution algorithm, 16,711 genes were available for differential analysis.

Before deconvolution, 341 genes were differentially expressed (FDR < 0.05) between the ICMandTE and the TE_part (Figure 3A). After deconvolution, comparison between DeMixT_ICM_cells and DeMixT_TE_cells yielded 7,565 differentially expressed genes while the comparison DeMixT_ICM_cells *vs* TE_part yielded 6,085 differentially expressed genes, with 5,925 in common (72%). Moreover, except one of the initially 341 differentially expressed genes before deconvolution, were also identified as differentially expressed in both post-deconvolution analyses. On the PCA graphic of individuals, ICMandTE and TE_part were not really separated before deconvolution (Figure 3B). DeMixT_TE_cells and TE_part were partly superposed, suggesting that datasets before and after deconvolution have a

bioRxiv preprint doi: https://doi.org/10.1101/2021.04.07.438786; this version posted April 9, 2021. The copyright holder for this preprint (which was not certified by peer review) is the author/funder, who has granted bioRxiv a license to display the preprint in perpetuity. It is made available under aCC-BY-NC-ND 4.0 International license.

similar global gene expression; whereas the DeMixT_ICM_cells group is clearly separated from both on Axis 2 (14.3% of variance), indicating that the deconvolution effectively enabled the separation of gene expression in the two cell types.

Six of the 12 genes previously identified as more expressed in ICM [23] were also more expressed in ICMandTE *vs* TE_part comparison (Table 2). After deconvolution (comparison DeMixT_ICM_cells *vs* TE_part), 3 more genes previously identified were also differentially expressed. However, for two of them (*POU Class 5 Homeobox 1*, *POU5F1* and *Undifferentiated Embryonic Cell Transcription Factor 1*, *UTF1*), their expression was increased in TE_part after deconvolution. In TE, any genes previously identified were differentially expressed in the comparison ICMandTE *vs* TE_part, *i.e.*, before deconvolution. After deconvolution, the expression of 2 genes was increased in TE_part compared to DeMixT_ICM_cells.

Table 2: Comparison of selected genes expression before and after deconvolution

	Gene name	Ensembl ID	ICMandTE *vs* TE_part		DeMixT_ICM_cells *vs* TE_part	
			log2FC from DeSeq2	padj	log2FC from DeSeq2	padj
ICM	**SOX2**	ENSECAG00000010653	4.49	0.02	6.49	1.7E-06
	NANOG	ENSECAG00000012614	4.24	1.0E-07	5.98	2.4E-15
	SPP1	ENSECAG00000017191	4.02	8.4E-09	5.74	5.1E-16
	LIN28B	ENSECAG00000020994	3.23	1.3E-10	5.00	4.7E-22
	SMARCA2	ENSECAG00000024187	0.62	0.97	1.25	0.07
	POU5F1 (OCT4)	ENSECAG00000008967	0.60	0.009	-2.04	4.6E-07
	ID2	ENSECAG00000008738	0.44	0.29	1.24	9.0E-05
	DNMT3B	ENSECAG00000012102	0.35	0.24	0.8	0.06
	DPPA4	ENSECAG00000013271	0.35	0.04	1.14	1.8E-05
	SALL4	ENSECAG00000018533	0.10	1	0.60	0.01
	KLF4	ENSECAG00000010613	-0.04	1	-0.81	0.39
	UTF1	ENSECAG00000039888	-0.13	1	-2.21	7.3E-05

bioRxiv preprint doi: https://doi.org/10.1101/2021.04.07.438786; this version posted April 9, 2021. The copyright holder for this preprint (which was not certified by peer review) is the author/funder, who has granted bioRxiv a license to display the preprint in perpetuity. It is made available under aCC-BY-NC-ND 4.0 International license.

TE	**TFAP2A**	ENSECAG00000017468	-0.17	0.46	-0.30	0.004
	CDX2	ENSECAG00000027754	-0.14	0.77	-0.23	0.07
	ELF3	ENSECAG00000014608	-0.13	1	-0.19	0.27
	GATA2	ENSECAG00000016768	-0.13	1	-0.29	0.048
	GATA3	ENSECAG00000024574	-0.10	0.87	-0.05	0.64
	TEAD4	ENSECAG00000011303	-0.10	0.96	0.00	1
	FREM2	ENSECAG00000020410	0.07	1	0.19	0.44

Gene expressions were obtained from RNA of 11 equine embryos bissected in two hemi-embryos: one part is composed only of trophoblast (TE), TE_part, while the other part is composed of TE and inner cell mass (ICM), ICMandTE. As it is impossible to estimate the proportion of each cells in ICMandTE, deconvolution algorithm (package DeMixT) was used to estimate gene expression of these different kind of cells. DeMixT_ICM_cells dataset is the deconvoluted gene expression of ICM cells from ICMandTE. Log2 fold change (log2FC) and padj (adjusted p-value with Benjamini-Hochberg correction) were obtained with Deseq2 package. TE_part is the reference group in both analyses: when log2 fold changes (log2FC) > 0, gene is more expressed in ICMandTE or DeMixT_ICM_cells while when log2FC < 0, gene is more expressed in TE_part. Green is used to represent gene differentially expressed in the present study. Orange is used to represent gens that have been previously identified as predominant in the ICM [23] but which are identified here as predominant in the TE.

For further analysis, DeMixT_ICM_cells and TE_part gene expression datasets are presented. Nevertheless, the comparison of maternal age on ICMandTE dataset (graphics, differential gene expression analysis and GSEA) was also performed and this analysis is available in Additional file 2, 3 and 4.

Differential gene expression in deconvoluted ICM cells' genes expression according to maternal age

bioRxiv preprint doi: https://doi.org/10.1101/2021.04.07.438786; this version posted April 9, 2021. The copyright holder for this preprint (which was not certified by peer review) is the author/funder, who has granted bioRxiv a license to display the preprint in perpetuity. It is made available under aCC-BY-NC-ND 4.0 International license.

After filtering out of genes with an average expression < 10 counts/maternal age group/hemi-embryo, 13,735 genes were considered as expressed in the ICM cells from OM or YM embryos including 255 differentially expressed genes (227 downregulated and 28 upregulated in OM) (Figure 4A and Additional file 5). Only 218 and 12 genes out of the down- and upregulated genes, respectively, were associated to a known protein in human. These downregulated genes in ICM of embryos from OM mainly belonged to cellular process, metabolic process and biological regulation in GO biological process gene sets (Figure 4A). From downregulated genes in OM ICM, 84 pathways were statistically overrepresented in GO Biological process leading to 16 most specific subclass pathways according to hierarchy sorting by PANTHER (Figure 4B). Overrepresented pathways in downregulated genes in OM ICM were linked to cell division, embryo morphogenesis, histone methylation, protein modification processes and cytoskeleton organization.

Upregulated DEGs in OM ICM were mainly part of biological regulation, response to stimulus, cellular process, signaling and metabolic process in GO biological process gene sets (Figure 4A). No pathway was statistically overrepresented in upregulated genes in ICM of embryos from old mares using PANTHER overrepresentation testing.

Differential gene expression in pure TE part gene expression

In the TE, 13,178 genes were considered as expressed in OM or YM. Fourteen were differentially expressed (Additional file 6) with 11 genes being downregulated and 3 being up regulated in OM (Figure 4A). Only 12 genes were associated to a known protein in human. Downregulated genes in OM mainly belonged to both cellular and metabolic process in GO biological process gene sets.

Gene set enrichment analysis in deconvoluted ICM cells' genes expression according to maternal age

After Entrez Gene ID conversion, 12,344 genes were considered expressed in ICM. In the GO Biological Process database, 106 identified gene sets differed according to maternal age in the ICM (11 enriched

bioRxiv preprint doi: https://doi.org/10.1101/2021.04.07.438786; this version posted April 9, 2021. The copyright holder for this preprint (which was not certified by peer review) is the author/funder, who has granted bioRxiv a license to display the preprint in perpetuity. It is made available under aCC-BY-NC-ND 4.0 International license.

443 in OM and 95 enriched in YM) (Additional file 7). In the KEGG database, 14 gene sets were perturbed
444 (Additional file 7).
445 Using SUMER analysis (Figure 5), gene sets enriched in OM ICM were mainly grouped under terms
446 “Respiratory electron transport chain” and “Translational elongation”. The first term represents
447 mitochondrial function while the second represents translation function. Moreover, terms relative to
448 “Systemic lupus erythematosus” are conserved by SUMER analysis and enriched in OM ICM. Genes
449 involved in these enrichments were also present in dysregulated metabolic pathways.
450 Gene sets enriched in YM ICM were involved in different biological processes such as “Mitotic nuclear
451 division” which is relative to mitosis. Under this term, “Spindle organization” and “Negative regulation
452 of supramolecular fiber organization” terms represent the assembly of spindle during mitosis.
453 “Chromosome segregation” is also found in this grouping. Furthermore, terms under “Golgi vesicle
454 transport” seem to be involved in cytokinesis and vesicle trafficking. The catabolism of protein and
455 mRNA is represented by “Ubiquitin mediated proteolysis”. Translation function is represented by
456 several terms grouped under “covalent chromatin modification” in the mitosis part.
457 “Leukocyte transendothelial migration” term is also enriched in YM ICM and seems to represent cell
458 signaling and adhesion. Indeed, this term regroups several pathways such as “Focal adhesion”,
459 “Adherens junction” and “WNT signaling pathway”.
460 Finally, further terms related to embryo development could be found in different groups such as
461 “Dendrite development”, “Cell differentiation in spinal cord” or “endothelial cell development”.
462
463 *Gene set enrichment analysis in TE*
464 After Entrez Gene ID conversion, 11,874 genes were considered expressed in TE from OM or YM
465 embryos. In GO BP database, 38 gene sets were perturbed by mares’ age in the TE of embryos (11
466 enriched in YM and 27 enriched in OM) (Additional file 8). In the KEGG database, 5 pathways were
467 enriched in the TE of OM embryos (Additional file 8).

bioRxiv preprint doi: https://doi.org/10.1101/2021.04.07.438786; this version posted April 9, 2021. The copyright holder for this preprint (which was not certified by peer review) is the author/funder, who has granted bioRxiv a license to display the preprint in perpetuity. It is made available under aCC-BY-NC-ND 4.0 International license.

As in ICM part, using SUMER analysis, translation (represented by both "Translational termination" and "Ribosome" terms) and mitochondrial function (represented by "Oxidative phosphorylation" associated terms) were enriched in OM embryos. "Proteasome" term is enriched in OM embryos representing protein catabolism.

Moreover, transcription (represented by "Peptidyl lysine trimethylation" term) and embryo development (represented by "spinal cord development") were, as in ICM, also, enriched in YM embryos. Finally, in TE, "Regulation of action potential" term and associated terms were enriched in YM. These terms could be related to ion movement.

Discussion

Maternal aging did not affect embryo recovery rate, embryo size nor total RNA quantity. Moreover, total RNA content in equine embryo was exponentially linked to embryo diameter and was not affected by maternal age.

As in tumor, today, the only way to analyze separate expression of ICM and TE cells in mammalian embryos is to use micromanipulation but micromanipulation is expensive in time and requires adapted skills and material. In this study, micromanipulation to properly separate ICM and TE was not possible. Therefore, deconvolution appears to be a good option to analyze the effects of maternal ICM gene expression in mixed ICM and TE samples. Deconvolution seemed to have been effective on embryo to separate ICM and TE gene expression. Indeed, the 341 genes differentially expressed in ICMandTE *vs* TE_part were also identified by comparing TE with post-deconvolution ICM cells gene expression dataset. Moreover, after deconvolution, more genes were differentially expressed between TE and ICM datasets and among them, more genes identified in literature were differentially expressed. Finally, PCA showed that deconvolution separate DeMixT_ICM_cells from other datasets while before deconvolution ICMandTE and TE_part were partly superposed. Only POU5F1 and UTF1 differed in terms of allocation between previously published data [23] and the present study. In data before deconvolution, expression of POU5F1 and UTF1 were extremely variable according to embryo

bioRxiv preprint doi: https://doi.org/10.1101/2021.04.07.438786; this version posted April 9, 2021. The copyright holder for this preprint (which was not certified by peer review) is the author/funder, who has granted bioRxiv a license to display the preprint in perpetuity. It is made available under aCC-BY-NC-ND 4.0 International license.

494 diameter in both compartments. Deconvolution reduced the variability of both gene expression in ICM
495 but not in TE. Studies showed that POU5F1 is expressed in both compartments until Day 10 post
496 ovulation in equine in vivo produced embryos [47] but its expression decreases progressively from Day
497 7 in TE cells. Thus, the statistically increased expression of POU5F1 in TE on Day 8 is compatible with
498 previously published data.
499 Therefore, it was chosen to only present the analysis of the effects of age in DeMixT_ICM_cells dataset.
500 In all cases, deconvolution did not change the principal results of maternal aging on embryo gene
501 expression because the comparison of maternal age in ICMandTE and DeMixT_ICM_cells gave
502 comparable results.
503 In both ICM and TE, the expression of genes involved in mitochondrial function and translation with
504 ribosome biogenesis were enriched in OM embryos while transcription with chromatin modification
505 was enriched in YM embryos (Figure 6). Mitosis, signaling and adhesion pathways were additionally
506 altered and the expression of genes involved in embryo development was particularly reduced in the
507 ICM hemi-embryos from old mares. Finally, in the TE, ion movement related genes were affected.
508 Several studies on mature oocytes in women and mice, using microarrays and RNAseq, had shown a
509 differential expression of genes involved in mitochondrial, cell cycle, cytoskeleton functions and
510 related pathways according to maternal age [48–50], as observed in the present study in equine
511 blastocysts, especially in the ICM. In equine follicles and oocytes, gene expression, as studied by RT-
512 qPCR, quantitatively and temporally differed with maternal age, suggesting a desynchronization of
513 essential genes for maturation [51]. Moreover, a study on the expression of 48 genes in cumulus-
514 oocytes complexes from young (< 12 years of age) and old (> 18 years old) mares showed differential
515 expression that may be related with the reduced developmental competence observed in old mares'
516 oocytes [52]. Finally, genes related to mitochondrial replication and function were down-regulated in
517 oocytes of old mares [16]. Even effects of maternal aging on gene expression in equine oocytes, using
518 high throughput techniques, are not yet available, results on equine Day 8 blastocysts suggest that
519 mitochondrial perturbations present in the oocyte persist until the blastocyst stage. In humans, single-

bioRxiv preprint doi: https://doi.org/10.1101/2021.04.07.438786; this version posted April 9, 2021. The copyright holder for this preprint (which was not certified by peer review) is the author/funder, who has granted bioRxiv a license to display the preprint in perpetuity. It is made available under aCC-BY-NC-ND 4.0 International license.

520 embryo RNA-seq analysis showed that maternal aging alters the transcriptome of blastocysts derived
521 from ICSI. Genes altered by maternal age were related to segregation of chromosomes, embryonic
522 growth and cell signaling [53,54], as observed in our study on equine blastocysts.
523 The equine embryo remains spherical, grows very fast and is surrounded by its glycoprotein capsule
524 up to 22 days post ovulation [55]. At 8 days post ovulation, equine embryos are therefore growing and
525 the endodermal layer entirely delineates the future yolk sac (Figure 6) [56]. Moreover, whereas in Day
526 7 embryos, the epiblast is lined by a continuous layer of trophoblast named the polar trophoblast. As
527 the blastocyst grows, epiblast cells phagocyte polar trophoblast cells that become discontinuous.
528 During this time, epiblast and polar trophoblast cells divided and are bound by tight junctions [57]. The
529 turnover in focal adhesion is essential for cell movement and phagocytosis [58].
530 Cell signaling and adhesion function were altered in OM embryos. Indeed, KEGG pathways "focal
531 adhesion" and "adherens junction" regrouped in “Leukocyte transendothelial migration” on Figure 4
532 are disturbed in old mares' embryos. Focal adhesions are subcellular structures observed in adherent
533 cells, that are clusters of different structural and signaling molecules and integrins that form a physical
534 link between the actin cytoskeleton and the extracellular matrix [59,60]. Integrins are the major
535 receptors for cell adherence to extracellular matrix proteins in focal adhesions. Indeed, they play an
536 important role in transmembrane connections to the cytoskeleton and activation of several signaling
537 pathways, as growth factor receptors [61]. *Integrin Subunit Alpha V* (*ITGAV*) expression was reduced
538 in the ICM (log2FC = -1.66; FDR < 0.05) of embryos collected from OM. In different human breast cancer
539 cell lines, cell proliferation, invasion and renewal are restricted when *ITGAV* is inhibited [62].
540 Therefore, the reduction of *ITGAV* could lead to an impaired cell signalization in OM embryos.
541 Moreover, small GTPases within the Rho family are required for the turnover of actin filaments and
542 cell adhesions necessary for cell migration, that are essential processes for the proper development of
543 the embryo. Activity and localization of each Rho GTPase must be precisely regulated as the
544 communication between them is indispensable to achieve this process [63]. The *Rho GTPase Activating*
545 *Protein 9* and *35* (*ARHGAP9* and *ARHGAP35*) were downregulated (respectively, log2FC = -1.83, FDR <

bioRxiv preprint doi: https://doi.org/10.1101/2021.04.07.438786; this version posted April 9, 2021. The copyright holder for this preprint (which was not certified by peer review) is the author/funder, who has granted bioRxiv a license to display the preprint in perpetuity. It is made available under aCC-BY-NC-ND 4.0 International license.

546 0.05 and log2FC = -0.74, FDR < 0.05) in OM ICM. *ARHGAP35* codes for P190 Rho GTPase activating
547 protein that mediates signalization through integrin-dependent adhesion in cells. Aberrant neural
548 morphogenesis, related to an accumulation of polymerized actin in embryoneural tube cells, is
549 reported in mice lacking P190 Rho GTPase activating proteins [64]. Furthermore, P21 activated kinases
550 (PAK) are effector kinases for other small Rho GTPases such as Rac and regulate the polymerization of
551 actin and can affect the microtubule organization and therefore the regulation of cytoskeleton [65].
552 Once activated by this signaling pathway, PAKs promote the turnover of focal adhesions. PAKs will
553 then, trigger p38 complex activation that regulates transcription [66]. *PAK3* was downregulated in the
554 OM ICM (log2FC = -3.76, FDR < 0.001). However, in TE, *SLIT-ROBO Rho GTPase Activating Protein 3,*
555 *SRGAP3* was one of the upregulated genes in OM (log2FC = 2.52, FDR < 0.01). This gene regulates
556 cytoskeletal reorganization and plays an important role in the formation of cell-cell adhesion [67].
557 Therefore, maternal aging seems to alter focal adhesion in both ICM and TE of embryos but, while in
558 ICM, it seems to reduce cohesion and signalization, in TE it seems to reinforce them.
559 Several signaling pathways required for development were altered and numerous genes related to
560 focal adhesions and signaling pathways were down-regulated in OM ICM (*ARHGAP9* and *ARHGAP35*;
561 *B-Raf Proto-Oncogene, Serine/Threonine Kinase*, *BRAF*; *Filamin C*, *FLNC*; *FYN Proto-Oncogene, Src*
562 *Family Tyrosine Kinase*, *FYN*; *PAK3*; *Protein Phosphatase 1 Regulatory Subunit 12A*, *PPP1R12A*; *Talin 2*,
563 *TLN2*; *X-Linked Inhibitor Of Apoptosis*, *XIAP*). Among all signaling pathways, transforming growth factor
564 beta (TGF-β), Wg et Int (Wnt), mitogen-activated protein kinases (MAPK) and apoptosis signaling were
565 altered by maternal age in equine embryos. Indeed, *transforming growth factor beta receptor 1*
566 (*TGFBR1*) was downregulated (log2FC = -4.34; FDR < 0.05) in the ICM of embryos from old mares.
567 *TGFBR1* is one of the two dimers for the receptor for transforming growth factors beta. This factor
568 family is essential in the generation of axes and cell fate commitment during mammal embryogenesis
569 [68]. Therefore, the reduced production of TGF-β receptor in ICM could impair the establishment of
570 cell lines in old mares' embryos. Moreover, *Casein Kinase 1 Alpha 1*, (*CSNK1A1*) and *Protein*
571 *Phosphatase 2 Regulatory Subunit B'Epsilon* (*PPP2R5E*), involved in Wnt signaling pathway, were

bioRxiv preprint doi: https://doi.org/10.1101/2021.04.07.438786; this version posted April 9, 2021. The copyright holder for this preprint (which was not certified by peer review) is the author/funder, who has granted bioRxiv a license to display the preprint in perpetuity. It is made available under aCC-BY-NC-ND 4.0 International license.

572 downregulated in OM embryos. Wnt signaling pathway is also involved in nervous development
573 system and may act on cell determination in mice embryos [69]. In horses, gastrulation begins by Day
574 12 post ovulation and the primitive streak develops quickly after mesoderm formation [70]. It is
575 therefore possible that the alteration of the Wnt signaling pathway could have a negative impact on
576 the brain development of the future fetus. This hypothesis could be confirmed by the fact that *DMRT3*
577 (*Doublesex And Mab-3 Related Transcription Factor 3*) was downregulated in the OM ICM (log2FC = -
578 3.07, FDR < 0.05). DMRT3 is required for the proper development of the brain in prenatal chicken and
579 mice [71]. Moreover, mutations of this gene are responsible for different gaits in horses (specific to
580 aptitude to trot instead of cantering) [72]. Therefore, altogether, the data indicate that cell fate
581 commitment in ICM seems to be altered by maternal aging.
582 Cell cycle related pathways and genes are also disturbed by maternal aging. Indeed, the expression of
583 *Pleckstrin Homology domain-Interacting Protein* (*PHIP*), also known as replication initiation
584 determinant, was reduced (log2FC = -0.86, FDR < 0.01) in the OM ICM. This gene is required for the
585 initiation of DNA replication. Fibroblasts originated from mice embryos with depleted *PHIP* expression
586 presented less replication-initiation as well as abnormal replication fork progression events [73].
587 Moreover, several cyclins (CCN) were less expressed in the ICM of embryos from old mares (*CCNB3*,
588 *CCNI* and *CCNT2*). Cyclins are key cell cycle regulators and, for instance cyclin B3 degradation allows
589 the passage from metaphase (chromatids aligned on metaphase plate) to anaphase (segregation of
590 sister chromatids) [74]. During metaphase and anaphase, spindle assembly and chromosome
591 segregation could also be compromised. Indeed, genes involved in the formation of microtubules
592 (*Tubulin Gamma 2*, *TUBG2*) [75], the generation of the mitotic spindle (*Never in Mitosis A related kinase*
593 *9*, *NEK9*) [76], the production of cohesion and condensing complexes (*Structural Maintenance Of*
594 *Chromosomes 4*, *SMC4*) [77], the control of centriole length, important for centrosomes and
595 microtubules organization (*Centriolar Coiled-Coil Protein 110*, *CCP110*) [78], the amplification of intra-
596 spindle microtubules allowing the formation of a sufficient quantity of kinetochore (*HAUS Augmin Like*
597 *Complex Subunit 6*, *HAUS6*) [79], the stabilization and protection of the cohesin complex association

bioRxiv preprint doi: https://doi.org/10.1101/2021.04.07.438786; this version posted April 9, 2021. The copyright holder for this preprint (which was not certified by peer review) is the author/funder, who has granted bioRxiv a license to display the preprint in perpetuity. It is made available under aCC-BY-NC-ND 4.0 International license.

598 with chromatin (*Cell Division Cycle Associated 5*, *CDCA5*; *shugosin 2*, *SGO2*) [80,81] and the production
599 of microtubule-based motor proteins (*Kinesin Family Member 14* and *23*, *KIF14* and *KIF23*) [82] were
600 downregulated in OM ICM. Furthermore, *Centromere protein F* (*CENPF*, log2FC = -1.11, FDR < 0.0001),
601 an important regulator of chromosome segregation during mitosis, was reduced in OM ICM. CENPF is
602 indispensable for murine embryo development from the first stages of development until at least the
603 blastocyst stage [83]. Impaired CENPF expression could induce chromosome mis-segregation in the
604 ICM of old mares' embryos.
605 Cytokinesis seems to also be altered by maternal age. *CD2-associated protein* (*CD2AP*) and *Vacuolar*
606 *Protein Sorting 4 Homolog A* (*VPS4A*) were downregulated in OM ICM (respectively, log2FC = -0.90,
607 FDR < 0.05 and log2FC = -0.77, FDR < 0.05). Both are involved in the late phase of cytokinesis which
608 correspond to the abscission of the cell, producing two daughter cells [84,85]. Globally, results suggest
609 that cell division is impaired or indicate that there is less division in the ICM of old mares' embryos.
610 Transcription is regulated by epigenetic marks. Several pathways linked to methylation and acetylation
611 were enriched in YM ICM and TE in relation to numerous upregulated genes in YM ICM (i.e., *Histone*
612 *Deacetylase 1* and *2*, *HDAC1* and *HDAC2*; *Helicase, Lymphoid Specific*, *HELLS*; *DNA Methyltransferase 3*
613 *Alpha*, *DNMT3A*; *Lysine Acetyltransferase 6B*, *KAT6B*; *Lysine Demethylase 4A*, *KDM4A*; *Lysine*
614 *Methyltransferase 2A*, *KMT2A*; *Nuclear Receptor Binding SET Domain Protein 3*, *NSD3*; *SET Domain*
615 *Containing 5*, *SETD5*; *Tet Methylcytosine Dioxygenase 1*, *TET1*). At blastocyst stage, *de novo*
616 methylation is more important in the inner cell mass than in trophoblast cells and is essential for the
617 proper development of mammalian embryos [86]. *DNMT3A* is essential for *de novo* methylation and
618 required for embryo viability [87]. *DNMT3A* expression was reduced in OM ICM (log2FC = -1.01, FDR <
619 0.05). As it has been shown that maternal aging increases the acetylation of lysine 12 of histone H4 in
620 mice oocytes, affecting fertilization and embryo development [88], it is likely that the methylation and
621 acetylation dysregulation observed in the embryos of old mares could be inherited from the oocyte
622 rather than directly due to embryo environment.

bioRxiv preprint doi: https://doi.org/10.1101/2021.04.07.438786; this version posted April 9, 2021. The copyright holder for this preprint (which was not certified by peer review) is the author/funder, who has granted bioRxiv a license to display the preprint in perpetuity. It is made available under aCC-BY-NC-ND 4.0 International license.

623 Many of the perturbed gene sets were involved in protein metabolism. In OM ICM, translation was
624 enriched but protein catabolism is not, whilst in TE, both are enriched. The biogenesis of ribosomes
625 and protein metabolism regulation are crucial for embryo development. Still in the ICM, proteasome
626 and mRNA catabolism pathways were also affected. In embryonic stem cells, the proteasome plays a
627 role in the restriction of permissive transcriptional activity by promoting a dynamic turnover of
628 transcription factors [89].
629 Both in OM ICM and TE, several pathways related to mitochondrial function were enriched.
630 Mitochondria are long known to be the "powerhouse" of cells, producing most of the necessary ATP
631 for cellular function [90]. ATP production is possible through oxidative phosphorylation enabled by the
632 electron transport chain in the inner membrane of mitochondria. This process begins with the
633 oxidation of NADH or FADH that generates a proton gradient across the mitochondrial membrane,
634 driving ATP synthesis through the phosphorylation of ADP *via* ATPase [91]. Enriched pathways in OM
635 embryos demonstrate that the NADH dehydrogenase (complex I), the oxidoreductase acting on a
636 heme group of donors (complex III) with the global electron carrier, and the proton-transporting ATP
637 synthase (1^{rst} part of the complex V) activities were particularly enriched while the second part of
638 complex V is depleted. Since all complexes are required to produce ATP, the impaired complex
639 generation may lead to mitochondrial stress and uncoupled respiratory chain, resulting in poor ATP
640 production. In human IVF embryos, reduced mitochondrial respiration efficiency, with a negative effect
641 on embryo development, is observed when oocytes are collected from old women [92]. In mammalian
642 expanded blastocysts, energy requirement is high, probably because of the need for ion transport
643 enabling quick blastocoel cavity expansion. Defects in metabolic requirements during blastocyst
644 development are associated with impaired implantation [93]. Equine embryos are not an exception
645 [94].
646 Mitochondria being maternally inherited, uncoupling of the mitochondrial respiratory chain may
647 originate from mitochondrial defects already present in oocytes [95]. Studies have shown that, in
648 human, poor oocyte quality is responsible for the decline in fertility associated with maternal aging.

bioRxiv preprint doi: https://doi.org/10.1101/2021.04.07.438786; this version posted April 9, 2021. The copyright holder for this preprint (which was not certified by peer review) is the author/funder, who has granted bioRxiv a license to display the preprint in perpetuity. It is made available under aCC-BY-NC-ND 4.0 International license.

649 The reduced oocyte developmental competence in older women is related to mitochondrial
650 dysfunction [96]. Regardless of the cell type, it is well known that mitochondrial DNA is more sensitive
651 to mutation than nuclear DNA and that aging is an important risk factor. In mammalian oocytes,
652 mitochondrial DNA mutations increase with age and are inversely correlated with oocyte quality [97–
653 99]. In mice, oocyte mitochondrial DNA content increases during *in vivo* oogenesis without difference
654 according to mice age [100]. In horses' oocytes, before *in vitro* maturation, no difference between
655 young and old mares is observed while after, reduced mitochondrial DNA copy numbers, increased
656 swelling and reduced mitochondrial cristae are reported in oocytes collected from mares >12 years.
657 This suggests that oocyte mitochondria from old mares present deficiencies that become problematic
658 when energy needs are high, as during *in vitro* maturation or subsequent embryo development [101].
659 Because mitochondrial replication in equine embryos does not begin until the blastocyst stage [102],
660 oocyte mitochondrial numerical or functional deficiencies may compromise early embryogenesis.
661 Alternatively, perturbations in mitochondrial gene expression as observed in old mares' embryos may
662 also result from alterations of the maternal environment. Indeed, mitochondrial function can be
663 improved in mouse embryos by adding antioxidants to the *in vitro* culture medium [103]. To our
664 knowledge, there is no study on oviductal or uterine fluid composition according to maternal age at
665 least in the horse, at the present time.
666 Finally, ATP production defects could affect embryo blastocoel expansion. Indeed, in TE, the GO
667 biological process "Regulation of action potential" and "Transmission nerve impulse", related to ion
668 movement, were enriched in YM embryos. These processes are associated with genes involved in the
669 action potential dependent ion channels. These ion channels such as NA^+, K^+, ATPase are essential for
670 the accumulation of blastocoel and subsequently yolk sac fluid in equine embryos [104]. Their
671 inhibition is detrimental for embryo development [105]. Thus, both reduced ATP production and
672 disturbed ion channels' function may impact embryo growth. Studies on blastocyst growth and size
673 according to mares' age, however, are controversial [9–15], probably due to the fact that the size of
674 the embryo at the same stage is very variable, as it is the case in this study. To this time, no study on

bioRxiv preprint doi: https://doi.org/10.1101/2021.04.07.438786; this version posted April 9, 2021. The copyright holder for this preprint (which was not certified by peer review) is the author/funder, who has granted bioRxiv a license to display the preprint in perpetuity. It is made available under aCC-BY-NC-ND 4.0 International license.

675 the effect of mares' age on equine NA^+, K^+, ATPase abundance and function in equine embryos is
676 available.
677 Altogether these data indicate that several processes related to chromatin segregation, cytokinesis,
678 apposition of epigenetic marks and mitochondrial function are affected in older mares' embryos and
679 that the ICM appears to be more affected than the TE. These perturbations most certainly contribute
680 to the increased subfertility and early embryo loss observed in aged mares [2,6,7]
681

682 Conclusion

683 This is the first study showing an effect of maternal age on gene expression in the equine blastocyst at
684 Day 8 post ovulation. Maternal age, even for mares as young as 10 years old, disturbs mitosis,
685 translation and transcription, cell signaling and adhesion as well as mitochondrial function and cell
686 commitment in horse embryos. These perturbations on Day 8 post ovulation may affect the further
687 development of the embryo and as a result, may contribute to decreased fertility due to aging. Even if
688 the oocyte seems to be in great part responsible for these alterations, maternal environment could
689 also be responsible. So far, maternal age does not appear to have an impact on foal morphology at
690 birth but, as for placental function, more subtle effects may exist. Here, as embryos were collected
691 long before implantation, it is impossible to know if these embryos would have implanted and if they
692 would have produced a live foal or not. Studies on long-term growth and health of foals born to the
693 same mares are currently being performed.
694

695 List of abbreviations

696 ARHGAP35: Rho GTPase Activating Protein 35

697 ARHGAP9: Rho GTPase Activating Protein 9

698 BRAF: B-Raf Proto-Oncogene, Serine/Threonine Kinase

bioRxiv preprint doi: https://doi.org/10.1101/2021.04.07.438786; this version posted April 9, 2021. The copyright holder for this preprint (which was not certified by peer review) is the author/funder, who has granted bioRxiv a license to display the preprint in perpetuity. It is made available under aCC-BY-NC-ND 4.0 International license.

699 CCN: cyclin

700 CCP110: Centriolar Coiled-Coil Protein 110

701 CD2AP: CD2-associated protein

702 CD69: CD69 Molecule

703 CDCA5: Cell Division Cycle Associated 5

704 CENPF: Centromere protein F

705 CSNK1A1: Casein Kinase 1 Alpha 1

706 DEG: differential expressed genes

707 DeMixT_ICM_cells: deconvoluted gene expression in ICM cells

708 DeMixT_TE_cells: deconvoluted gene expression in TE cells

709 DMRT3: Doublesex And Mab-3 Related Transcription Factor 3

710 DNMT3A: DNA Methyltransferase 3 Alpha

711 ERR: embryo collection rate

712 FDR: false discovery rate

713 FLNC: Filamin C

714 FYN: FYN Proto-Oncogene, Src Family Tyrosine Kinase

715 GO BP: Gene Ontology biological process

716 GO: Gene Ontology

717 GSEA: gene set enrichment analyses

718 HAUS6: HAUS Augmin Like Complex Subunit 6

bioRxiv preprint doi: https://doi.org/10.1101/2021.04.07.438786; this version posted April 9, 2021. The copyright holder for this preprint (which was not certified by peer review) is the author/funder, who has granted bioRxiv a license to display the preprint in perpetuity. It is made available under aCC-BY-NC-ND 4.0 International license.

719 HDAC: Histone Deacetylase

720 HELLS: Helicase, Lymphoid Specific

721 ICM: inner cell mass

722 ICMandTE: inner cell mass enriched hemi-embryo

723 ICSI: intracytoplasmic sperm injection

724 ITGAV: Integrin Subunit Alpha V

725 KAT6B: Lysine Acetyltransferase 6B

726 KDM4A: Lysine Demethylase 4A

727 KEGG: Kyoto

728 KEGG: Kyoto Encyclopedia of Genes and Genomes

729 KIF: Kinesin Family Member

730 KMT2A: Lysine Methyltransferase 2A

731 Log2FC: log2 fold change

732 MAPK: mitogen-activated protein kinases

733 NEK9: Never in Mitosis A related kinase 9

734 NES: normalized enrichment score

735 NSD3: Nuclear Receptor Binding SET Domain Protein 3

736 OM: old mares

737 PAK: P21 activated kinases

738 PHIP: Pleckstrin Homology domain-Interacting Protein

bioRxiv preprint doi: https://doi.org/10.1101/2021.04.07.438786; this version posted April 9, 2021. The copyright holder for this preprint (which was not certified by peer review) is the author/funder, who has granted bioRxiv a license to display the preprint in perpetuity. It is made available under aCC-BY-NC-ND 4.0 International license.

PLAC8A: placenta Associated 8 A

POU5F1: POU Class 5 Homeobox 1

PPP1R12A: Protein Phosphatase 1 Regulatory Subunit 12A

PPP2R5E: Protein Phosphatase 2 Regulatory Subunit B'Epsilon

ROCK: Rho-associated coiled-coil kinases

RPS29: Ribosomal Protein S29

SETD5: SET Domain Containing 5

SGO2: shugosin 2

SMC4: Structural Maintenance Of Chromosomes 4

SRGAP3: SLIT-ROBO Rho GTPase Activating Protein 3

SRY: sex determining region Y

TE: trophoblast

TE_part: pure trophoblast hemi-embryo

TET1: Tet Methylcytosine Dioxygenase 1

TGF- β: transforming growth factor beta

TGFBR1: transforming growth factor beta receptor 1

TLN2: Talin 2

TUBG2: Tubulin Gamma 2

UTF1: Undifferentiated Embryonic Cell Transcription Factor 1

VPS4A: Vacuolar Protein Sorting 4 Homolog A

bioRxiv preprint doi: https://doi.org/10.1101/2021.04.07.438786; this version posted April 9, 2021. The copyright holder for this preprint (which was not certified by peer review) is the author/funder, who has granted bioRxiv a license to display the preprint in perpetuity. It is made available under aCC-BY-NC-ND 4.0 International license.

759 Wnt: Wg et Int

760 XIAP: X-Linked Inhibitor Of Apoptosis

761 XIST: X inactive Specific Transcript

762 YM: young mares

763

764 Bibliography

765 [1] Scoggin CF. Not just a number: effect of age on fertility, pregnancy and offspring vigour in
766 thoroughbred brood-mares. Reprod Fertil Dev 2015;27:872. https://doi.org/10.1071/RD14390.
767 [2] Allen WR, Brown L, Wright M, Wilsher S. Reproductive efficiency of Flatrace and National Hunt
768 Thoroughbred mares and stallions in England. Equine Veterinary Journal 2007;39:438–45.
769 https://doi.org/10.2746/042516407X1737581.
770 [3] Langlois B, Blouin C. Statistical analysis of some factors affecting the number of horse births in
771 France. Reprod Nutr Dev 2004;44:583–95. https://doi.org/10.1051/rnd:2004055.
772 [4] Ferreira JC, Canesin HS, Ignácio FS, Rocha NS, Pinto CR, Meira C. Effect of age and endometrial
773 degenerative changes on uterine blood flow during early gestation in mares. Theriogenology
774 2015;84:1123–30. https://doi.org/10.1016/j.theriogenology.2015.06.013.
775 [5] Ball BA, Little TV, Hillman RB, Woods GL. Pregnancy rates at Days 2 and 14 and estimated
776 embryonic loss rates prior to day 14 in normal and subfertile mares. Theriogenology
777 1986;26:611–9. https://doi.org/10.1016/0093-691X(86)90168-8.
778 [6] Chevalier-Clément F. Pregnancy loss in the mare. Animal Reproduction Science 1989;20:231–
779 44. https://doi.org/10.1016/0378-4320(89)90088-2.
780 [7] Souza JRM de, Gonçalves PBD, Bertolin K, Ferreira R, Ribeiro ASS, Ribeiro DB, et al. Age-
781 Dependent Effect of Foal Heat Breeding on Pregnancy and Embryo Mortality Rates in

bioRxiv preprint doi: https://doi.org/10.1101/2021.04.07.438786; this version posted April 9, 2021. The copyright holder for this preprint (which was not certified by peer review) is the author/funder, who has granted bioRxiv a license to display the preprint in perpetuity. It is made available under aCC-BY-NC-ND 4.0 International license.

Thoroughbred Mares. Journal of Equine Veterinary Science 2020;90:102982. https://doi.org/10.1016/j.jevs.2020.102982.

[8] Ball BA, Little TV, Weber JA, Woods GL. Survival of Day-4 embryos from young, normal mares and aged, subfertile mares after transfer to normal recipient mares. Reproduction 1989;85:187–94. https://doi.org/10.1530/jrf.0.0850187.

[9] Frank BL, Doddman CD, Stokes JE, Carnevale EM. Association of equine oocyte and cleavage stage embryo morphology with maternal age and pregnancy after intracytoplasmic sperm injection. Reprod Fertil Dev 2019;31:1812. https://doi.org/10.1071/RD19250.

[10] Panzani D, Rota A, Marmorini P, Vannozzi I, Camillo F. Retrospective study of factors affecting multiple ovulations, embryo recovery, quality, and diameter in a commercial equine embryo transfer program. Theriogenology 2014;82:807–14. https://doi.org/10.1016/j.theriogenology.2014.06.020.

[11] Carnevale EM, Bergfelt DR, Ginther OJ. Aging effects on follicular activity and concentrations of FSH, LH, and progesterone in mares. Animal Reproduction Science 1993;31:287–99. https://doi.org/10.1016/0378-4320(93)90013-H.

[12] Woods GL, Baker CB, Hillman RB, Schlafer DH. Recent studies relating to early embryonic death in the mare. Equine Veterinary Journal 1985;17:104–7. https://doi.org/10.1111/j.2042-3306.1985.tb04609.x.

[13] Carnevale EM, Ginther OJ. Defective Oocytes as a Cause of Subfertility in Old Mares. Biology of Reproduction 1995;52:209–14. https://doi.org/10.1093/biolreprod/52.monograph_series1.209.

[14] Camargo Ferreira J, Linhares Boakari Y, Sousa Rocha N, Saules Ignácio F, Barbosa da Costa G, de Meira C. Luteal vascularity and embryo dynamics in mares during early gestation: Effect of age and endometrial degeneration. Reprod Dom Anim 2019;54:571–9. https://doi.org/10.1111/rda.13396.

bioRxiv preprint doi: https://doi.org/10.1101/2021.04.07.438786; this version posted April 9, 2021. The copyright holder for this preprint (which was not certified by peer review) is the author/funder, who has granted bioRxiv a license to display the preprint in perpetuity. It is made available under aCC-BY-NC-ND 4.0 International license.

807 [15] Morel MCGD, Newcombe JR, Swindlehurst JC. The effect of age on multiple ovulation rates,
808 multiple pregnancy rates and embryonic vesicle diameter in the mare. Theriogenology
809 2005;63:2482–93. https://doi.org/10.1016/j.theriogenology.2004.09.058.
810 [16] Hendriks WK, Colleoni S, Galli C, Paris DBBP, Colenbrander B, Roelen BAJ, et al. Maternal age
811 and in vitro culture affect mitochondrial number and function in equine oocytes and embryos.
812 Reprod Fertil Dev 2015;27:957. https://doi.org/10.1071/RD14450.
813 [17] Chavatte-Palmer P, Velazquez MA, Jammes H, Duranthon V. Review: Epigenetics,
814 developmental programming and nutrition in herbivores. Animal 2018;12:s363–71.
815 https://doi.org/10.1017/S1751731118001337.
816 [18] Arnaud MG, Dubroeucq MH, Rivot MD. Notation de l'état corporel des chevaux de selle et de
817 sport: guide pratique. 1ère. Paris: Institut de l'élevage; 1997.
818 [19] Duchamp G, Bour B, Combarnous Y, Palmer E. Alternative solutions to hCG induction of
819 ovulation in the mare. J Reprod Fertil Suppl 1987;35:221–8.
820 [20] Bucca S, Carli A. Efficacy of human chorionic gonadotropin to induce ovulation in the mare,
821 when associated with a single dose of dexamethasone administered at breeding time: Efficacy
822 of human chorionic gonadotropin to induce ovulation when associated with dexamethasone.
823 Equine Veterinary Journal 2011;43:32–4. https://doi.org/10.1111/j.2042-3306.2011.00488.x.
824 [21] Martin M. Cutadapt removes adapter sequences from high-throughput sequencing reads.
825 EMBnet Journal 2011;17:10–2.
826 [22] Gutiérrez-Adán A, Perez-Crespo M, Fernandez-Gonzalez R, Ramirez M, Moreira P, Pintado B, et
827 al. Developmental Consequences of Sexual Dimorphism During Pre-implantation Embryonic
828 Development. Reprod Domest Anim 2006;41:54–62. https://doi.org/10.1111/j.1439-
829 0531.2006.00769.x.
830 [23] Iqbal K, Chitwood JL, Meyers-Brown GA, Roser JF, Ross PJ. RNA-Seq Transcriptome Profiling of
831 Equine Inner Cell Mass and Trophectoderm. Biology of Reproduction 2014;90.
832 https://doi.org/10.1095/biolreprod.113.113928.

bioRxiv preprint doi: https://doi.org/10.1101/2021.04.07.438786; this version posted April 9, 2021. The copyright holder for this preprint (which was not certified by peer review) is the author/funder, who has granted bioRxiv a license to display the preprint in perpetuity. It is made available under aCC-BY-NC-ND 4.0 International license.

[24] Beckelmann J, Budik S, Bartel C, Aurich C. Evaluation of Xist expression in preattachment equine embryos. Theriogenology 2012;78:1429–36. https://doi.org/10.1016/j.theriogenology.2012.05.026.

[25] Pertea M, Pertea GM, Antonescu CM, Chang T-C, Mendell JT, Salzberg SL. StringTie enables improved reconstruction of a transcriptome from RNA-seq reads. Nat Biotechnol 2015;33:290–5. https://doi.org/10.1038/nbt.3122.

[26] Robinson JT, Thorvaldsdóttir H, Winckler W, Guttman M, Lander ES, Getz G, et al. Integrative genomics viewer. Nat Biotechnol 2011;29:24–6. https://doi.org/10.1038/nbt.1754.

[27] Dobin A, Davis CA, Schlesinger F, Drenkow J, Zaleski C, Jha S, et al. STAR: ultrafast universal RNA-seq aligner. Bioinformatics 2013;29:15–21. https://doi.org/10.1093/bioinformatics/bts635.

[28] Liao Y, Smyth GK, Shi W. featureCounts: an efficient general purpose program for assigning sequence reads to genomic features. Bioinformatics 2014;30:923–30. https://doi.org/10.1093/bioinformatics/btt656.

[29] R Core Team. A Language and Environment for Statistical Computing. Vienna, Austria: R foundation for Statistical Computing; 2020.

[30] Rstudio Team. RStudio: Integrated Development for R. RStudio. Boston, USA: PBC; 2020.

[31] Pinheiro J, Bates D, Debroy S, Sarkar D, R Core Team. nlme: Linear and Nonlinear Mixed Effects Models. 2020.

[32] Giraudoux P. pgirmess: Spatial Analysis and Data Mining for Field Ecologists. 2018.

[33] Cao S, Wang JR, Ji S, Yang P, Chen J, Shen JP, et al. Differing total mRNA expression shapes the molecular and clinical phenotype of cancer. BioRxiv 2020:57. https://doi.org/10.1101/2020.09.30.306795.

[34] Wang Z, Cao S, Morris JS, Ahn J, Liu R, Tyekucheva S, et al. Transcriptome Deconvolution of Heterogeneous Tumor Samples with Immune Infiltration. IScience 2018;9:451–60. https://doi.org/10.1016/j.isci.2018.10.028.

bioRxiv preprint doi: https://doi.org/10.1101/2021.04.07.438786; this version posted April 9, 2021. The copyright holder for this preprint (which was not certified by peer review) is the author/funder, who has granted bioRxiv a license to display the preprint in perpetuity. It is made available under aCC-BY-NC-ND 4.0 International license.

[35] Love MI, Huber W, Anders S. Moderated estimation of fold change and dispersion for RNA-seq data with DESeq2. Genome Biol 2014;15:550. https://doi.org/10.1186/s13059-014-0550-8.

[36] Gómez-Rubio V. **ggplot2** - Elegant Graphics for Data Analysis (2nd Edition). J Stat Soft 2017;77. https://doi.org/10.18637/jss.v077.b02.

[37] Kassambara A, Mundt F. factoextra: Extract and Visualize the Results of Multivariate Data Analyses. 2020.

[38] Kolberg L, Raudvere U. gprofiler2: Interface to the "g:Profiler" Toolset. 2020.

[39] Yates AD, Achuthan P, Akanni W, Allen J, Allen J, Alvarez-Jarreta J, et al. Ensembl 2020. Nucleic Acids Research 2020;48:D682–8. https://doi.org/10.1093/nar/gkz966.

[40] Mi H, Ebert D, Muruganujan A, Mills C, Albou L-P, Mushayamaha T, et al. PANTHER version 16: a revised family classification, tree-based classification tool, enhancer regions and extensive API. Nucleic Acids Research 2021;49:D394–403. https://doi.org/10.1093/nar/gkaa1106.

[41] Subramanian A, Tamayo P, Mootha VK, Mukherjee S, Ebert BL, Gillette MA, et al. Gene set enrichment analysis: A knowledge-based approach for interpreting genome-wide expression profiles. Proceedings of the National Academy of Sciences 2005;102:15545–50. https://doi.org/10.1073/pnas.0506580102.

[42] Mootha VK, Lindgren CM, Eriksson K-F, Subramanian A, Sihag S, Lehar J, et al. PGC-1α-responsive genes involved in oxidative phosphorylation are coordinately downregulated in human diabetes. Nat Genet 2003;34:267–73. https://doi.org/10.1038/ng1180.

[43] Liberzon A, Birger C, Thorvaldsdóttir H, Ghandi M, Mesirov JP, Tamayo P. The Molecular Signatures Database Hallmark Gene Set Collection. Cell Systems 2015;1:417–25. https://doi.org/10.1016/j.cels.2015.12.004.

[44] Savage SR, Shi Z, Liao Y, Zhang B. Graph Algorithms for Condensing and Consolidating Gene Set Analysis Results. Molecular & Cellular Proteomics 2019;18:S141–52. https://doi.org/10.1074/mcp.TIR118.001263.

bioRxiv preprint doi: https://doi.org/10.1101/2021.04.07.438786; this version posted April 9, 2021. The copyright holder for this preprint (which was not certified by peer review) is the author/funder, who has granted bioRxiv a license to display the preprint in perpetuity. It is made available under aCC-BY-NC-ND 4.0 International license.

884 [45] Shannon P. Cytoscape: A Software Environment for Integrated Models of Biomolecular
885 Interaction Networks. Genome Research 2003;13:2498–504.
886 https://doi.org/10.1101/gr.1239303.
887 [46] McKinnon AO, Squires EL. Morphologic assessment of the equine embryo. Journal of the
888 American Veterinary Medical Association 1988;192:401–6.
889 [47] Hisey E, Ross PJ, Meyers SA. A Review of OCT4 Functions and Applications to Equine Embryos.
890 Journal of Equine Veterinary Science 2021;98:103364.
891 https://doi.org/10.1016/j.jevs.2020.103364.
892 [48] Grøndahl ML, Andersen CY, Bogstad J, Nielsen FC, Meinertz H, Borup R. Gene expression
893 profiles of single human mature oocytes in relation to age. Human Reproduction 2010;25:957–
894 68. https://doi.org/doi:10.1093/humrep/deq014.
895 [49] Reyes JM, Silva E, Chitwood JL, Schoolcraft WB, Krisher RL, Ross PJ. Differing molecular
896 response of young and advanced maternal age human oocytes to IVM. Human Reproduction
897 2017;32:2199–208. https://doi.org/10.1093/humrep/dex284.
898 [50] Hamatani T, Falco G, Carter MG, Akutsu H, Stagg CA, Sharov AA, et al. Age-associated alteration
899 of gene expression patterns in mouse oocytes. Human Molecular Genetics 2004;13:2263–78.
900 https://doi.org/10.1093/hmg/ddh241.
901 [51] Campos-Chillon F, Farmerie TA, Bouma GJ, Clay CM, Carnevale EM. Effects of aging on gene
902 expression and mitochondrial DNA in the equine oocyte and follicle cells. Reprod Fertil Dev
903 2015;27:925. https://doi.org/10.1071/RD14472.
904 [52] Cox L, Vanderwall DK, Parkinson KC, Sweat A, Isom SC. Expression profiles of select genes in
905 cumulus–oocyte complexes from young and aged mares. Reprod Fertil Dev 2015;27:914.
906 https://doi.org/10.1071/RD14446.
907 [53] Kawai K, Harada T, Ishikawa T, Sugiyama R, Kawamura T, Yoshida A, et al. Parental age and gene
908 expression profiles in individual human blastocysts. Sci Rep 2018;8:2380.
909 https://doi.org/10.1038/s41598-018-20614-8.

bioRxiv preprint doi: https://doi.org/10.1101/2021.04.07.438786; this version posted April 9, 2021. The copyright holder for this preprint (which was not certified by peer review) is the author/funder, who has granted bioRxiv a license to display the preprint in perpetuity. It is made available under aCC-BY-NC-ND 4.0 International license.

910 [54] McCallie BR, Parks JC, Trahan GD, Jones KL, Coate BD, Griffin DK, et al. Compromised global
911 embryonic transcriptome associated with advanced maternal age. J Assist Reprod Genet
912 2019;36:915–24. https://doi.org/10.1007/s10815-019-01438-5.
913 [55] Betteridge KJ, Eaglesome MD, MITCHELLt D, Flood PF, Beriault R. Development of horse
914 embryos up to twenty two days after ovulation: observations on fresh specimens. Journal of
915 Anatomy 1982;135:191–209.
916 [56] Enders AC, Schlafke S, Lantz KC, Liu IKM. Endoderm cells of the equine yolk sac from Day 7 until
917 formation of the definitive yolk sac placenta. Equine Veterinary Journal 1993;25:3–9.
918 https://doi.org/10.1111/j.2042-3306.1993.tb04814.x.
919 [57] Enders AC, Lantz KC, Liu IKM, Schlafke S. Loss of polar trophoblast during differentiation of the
920 blastocyst of the horse. Journal of Reproduction and Fertility 1988;83:447–60.
921 https://doi.org/10.1530/jrf.0.0830447.
922 [58] Hauck CR, Hsia DA, Schlaepfer DD. The Focal Adhesion Kinase--A Regulator of Cell Migration
923 and Invasion. IUBMB Life 2002;53:115–9. https://doi.org/10.1080/15216540211470.
924 [59] Provenzano PP, Keely PJ. Mechanical signaling through the cytoskeleton regulates cell
925 proliferation by coordinated focal adhesion and Rho GTPase signaling. Journal of Cell Science
926 2011;124:1195–205. https://doi.org/10.1242/jcs.067009.
927 [60] Zhao X, Guan J-L. Focal adhesion kinase and its signaling pathways in cell migration and
928 angiogenesis. Advanced Drug Delivery Reviews 2011;63:610–5.
929 https://doi.org/10.1016/j.addr.2010.11.001.
930 [61] Hynes, RO. Integrins: bidirectional, allosteric signaling machines. Cells 2002;110:673–87.
931 https://doi.org/10.1016/S0092-8674(02)00971-6.
932 [62] Cheuk IW-Y, Siu MT, Ho JC-W, Chen J, Shin VY. ITGAV targeting as a therapeutic approach for
933 treatment of metastatic breast cancer. American Journal of Cancer Research 2020;10:211–23.
934 [63] Riento K, Ridley AJ. ROCKs: multifunctional kinases in cell behaviour. Nat Rev Mol Cell Biol
935 2003;4:446–56. https://doi.org/10.1038/nrm1128.

bioRxiv preprint doi: https://doi.org/10.1101/2021.04.07.438786; this version posted April 9, 2021. The copyright holder for this preprint (which was not certified by peer review) is the author/funder, who has granted bioRxiv a license to display the preprint in perpetuity. It is made available under aCC-BY-NC-ND 4.0 International license.

936 [64] Brouns MR. p190 RhoGAP is required for neural development. Development 2000;127:4891–
937 903.
938 [65] Rane CK, Minden A. P21 activated kinases: Structure, regulation, and functions. Small GTPases
939 2014;5:e28003. https://doi.org/10.4161/sgtp.28003.
940 [66] Chan PM, Lim L, Manser E. PAK Is Regulated by PI3K, PIX, CDC42, and PP2Cα and Mediates
941 Focal Adhesion Turnover in the Hyperosmotic Stress-induced p38 Pathway. J Biol Chem
942 2008;283:24949–61. https://doi.org/10.1074/jbc.M801728200.
943 [67] Bacon C, Endris V, Rappold GA. The cellular function of srGAP3 and its role in neuronal
944 morphogenesis. Mechanisms of Development 2013;130:391–5.
945 https://doi.org/10.1016/j.mod.2012.10.005.
946 [68] Wu MY, Hill CS. TGF-β Superfamily Signaling in Embryonic Development and Homeostasis.
947 Developmental Cell 2009;16:329–43. https://doi.org/10.1016/j.devcel.2009.02.012.
948 [69] Kemp C, Willems E, Abdo S, Lambiv L, Leyns L. Expression of all Wnt genes and their secreted
949 antagonists during mouse blastocyst and postimplantation development. Dev Dyn
950 2005;233:1064–75. https://doi.org/10.1002/dvdy.20408.
951 [70] Gaivão MMF, Rambags BPB, Stout TAE. Gastrulation and the establishment of the three germ
952 layers in the early horse conceptus. Theriogenology 2014;82:354–65.
953 https://doi.org/10.1016/j.theriogenology.2014.04.018.
954 [71] Smith CA, Hurley TM, McClive PJ, Sinclair AH. Restricted expression of DMRT3 in chicken and
955 mouse embryos. Mechanisms of Development 2002;119:S73–6.
956 https://doi.org/10.1016/S0925-4773(03)00094-7.
957 [72] Andersson LS, Larhammar M, Memic F, Wootz H, Schwochow D, Rubin C-J, et al. Mutations in
958 DMRT3 affect locomotion in horses and spinal circuit function in mice. Nature 2012;488:642–6.
959 https://doi.org/10.1038/nature11399.

bioRxiv preprint doi: https://doi.org/10.1101/2021.04.07.438786; this version posted April 9, 2021. The copyright holder for this preprint (which was not certified by peer review) is the author/funder, who has granted bioRxiv a license to display the preprint in perpetuity. It is made available under aCC-BY-NC-ND 4.0 International license.

960 [73] Zhang Y, Huang L, Fu H, Smith OK, Lin CM, Utani K, et al. A replicator-specific binding protein
961 essential for site-specific initiation of DNA replication in mammalian cells. Nat Commun
962 2016;7:11748. https://doi.org/10.1038/ncomms11748.
963 [74] Yuan K, O'Farrell PH. Cyclin B3 Is a Mitotic Cyclin that Promotes the Metaphase-Anaphase
964 Transition. Current Biology 2015;25:811–6. https://doi.org/10.1016/j.cub.2015.01.053.
965 [75] Vinopal S, Černohorská M, Sulimenko V, Sulimenko T, Vosecká V, Flemr M, et al. γ-Tubulin 2
966 Nucleates Microtubules and Is Downregulated in Mouse Early Embryogenesis. PLoS ONE
967 2012;7:e29919. https://doi.org/10.1371/journal.pone.0029919.
968 [76] Fry AM, O'Regan L, Sabir SR, Bayliss R. Cell cycle regulation by the NEK family of protein kinases.
969 Journal of Cell Science 2012;125:4423–33. https://doi.org/10.1242/jcs.111195.
970 [77] Losada A, Hirano T. Shaping the metaphase chromosome: coordination of cohesion and
971 condensation. Bioessays 2001;23:924–35. https://doi.org/10.1002/bies.1133.
972 [78] Schmidt TI, Kleylein-Sohn J, Westendorf J, Le Clech M, Lavoie SB, Stierhof Y-D, et al. Control of
973 Centriole Length by CPAP and CP110. Current Biology 2009;19:1005–11.
974 https://doi.org/10.1016/j.cub.2009.05.016.
975 [79] Watanabe S, Shioi G, Furuta Y, Goshima G. Intra-spindle Microtubule Assembly Regulates
976 Clustering of Microtubule-Organizing Centers during Early Mouse Development. Cell Reports
977 2016;15:54–60. https://doi.org/10.1016/j.celrep.2016.02.087.
978 [80] Ladurner R, Kreidl E, Ivanov MP, Ekker H, Idarraga-Amado MH, Busslinger GA, et al. Sororin
979 actively maintains sister chromatid cohesion. EMBO J 2016;35:635–53.
980 https://doi.org/10.15252/embj.201592532.
981 [81] Rivera T, Losada A. Shugoshin and PP2A, shared duties at the centromere. Bioessays
982 2006;28:775–9. https://doi.org/10.1002/bies.20448.
983 [82] Welburn JPI. The molecular basis for kinesin functional specificity during mitosis. Cytoskeleton
984 2013;70:476–93. https://doi.org/10.1002/cm.21135.

bioRxiv preprint doi: https://doi.org/10.1101/2021.04.07.438786; this version posted April 9, 2021. The copyright holder for this preprint (which was not certified by peer review) is the author/funder, who has granted bioRxiv a license to display the preprint in perpetuity. It is made available under aCC-BY-NC-ND 4.0 International license.

985 [83] Zhou C-J, Wang X-Y, Han Z, Wang D-H, Ma Y-Z, Liang C-G. Loss of CENPF leads to developmental
986 failure in mouse embryos. Cell Cycle 2019;18:2784–99.
987 https://doi.org/10.1080/15384101.2019.1661173.
988 [84] Monzo P, Gauthier NC, Keslair F, Loubat A, Field CM, Marchand-Brustel YL, et al. Clues to CD2-
989 associated Protein Involvement in Cytokinesis□D □V. Molecular Biology of the Cell 2005;16:12.
990 [85] Babst M, Davies BA. Regulation of Vps4 During MVB Sorting and Cytokinesis. Traffic
991 2011;12:1298–305.
992 [86] Hales BF, Grenier L, Lalancette C, Robaire B. Epigenetic programming: From gametes to
993 blastocyst. Birth Defects Research Part A: Clinical and Molecular Teratology 2011;91:652–65.
994 https://doi.org/10.1002/bdra.20781.
995 [87] Marcho C, Cui W, Mager J. Epigenetic dynamics during preimplantation development.
996 REPRODUCTION 2015;150:R109–20. https://doi.org/10.1530/REP-15-0180.
997 [88] Suo L, Meng Q-G, Pei Y, Yan C-L, Fu X-W, Bunch TD, et al. Changes in acetylation on lysine 12 of
998 histone H4 (acH4K12) of murine oocytes during maternal aging may affect fertilization and
999 subsequent embryo development. Fertility and Sterility 2010;93:945–51.
1000 https://doi.org/10.1016/j.fertnstert.2008.12.128.
1001 [89] Szutorisz H, Georgiou A, Tora L, Dillon N. The Proteasome Restricts Permissive Transcription at
1002 Tissue-Specific Gene Loci in Embryonic Stem Cells. Cell 2006;127:1375–88.
1003 https://doi.org/10.1016/j.cell.2006.10.045.
1004 [90] Dumollard R, Duchen M, Carroll J. The Role of Mitochondrial Function in the Oocyte and
1005 Embryo. The mitochondrion in the germline and early development, vol. 77, Elsevier; 2007, p.
1006 21–49. https://doi.org/10.1016/S0070-2153(06)77002-8.
1007 [91] Balaban RS, Nemoto S, Finkel T. Mitochondria, Oxidants, and Aging. Cell 2005;120:483–95.
1008 https://doi.org/10.1016/j.cell.2005.02.001.

bioRxiv preprint doi: https://doi.org/10.1101/2021.04.07.438786; this version posted April 9, 2021. The copyright holder for this preprint (which was not certified by peer review) is the author/funder, who has granted bioRxiv a license to display the preprint in perpetuity. It is made available under aCC-BY-NC-ND 4.0 International license.

1009 [92] Wilding M, Dale B, Marino M, di Matteo L, Alviggi C, Pisaturo ML, et al. Mitochondrial
1010 aggregation patterns and activity in human oocytes and preimplantation embryos. Human
1011 Reproduction 2001;16:909–17. https://doi.org/10.1093/humrep/16.5.909.
1012 [93] Gardner DK, Harvey AJ. Blastocyst metabolism. Reprod Fertil Dev 2015;27:638.
1013 https://doi.org/10.1071/RD14421.
1014 [94] Lane M, O'Donovan MK, Squires EL, Seidel GE, Gardner DK. Assessment of metabolism of
1015 equine morulae and blastocysts. Mol Reprod Dev 2001;59:33–7.
1016 https://doi.org/10.1002/mrd.1004.
1017 [95] Hutchison CA, Newbold JE, Potter SS, Edgell MH. Maternal inheritance of mammalian
1018 mitochondrial DNA. Nature 1974;251:536–8. https://doi.org/10.1038/251536a0.
1019 [96] Krisher RL. Maternal age affects oocyte developmental potential at both ends of the age
1020 spectrum. Reprod Fertil Dev 2019;31:1. https://doi.org/10.1071/RD18340.
1021 [97] Yang L, Lin X, Tang H, Fan Y, Zeng S, Jia L, et al. Mitochondrial DNA mutation exacerbates female
1022 reproductive aging via impairment of the NADH/NAD $^{+}$ redox. Aging Cell 2020;19.
1023 https://doi.org/10.1111/acel.13206.
1024 [98] May-Panloup P, Boucret L, Desquiret-Dumas V, Ferré-L V, Morinière C, Descamps P, et al.
1025 Ovarian ageing: the role of mitochondria in oocytes and follicles. Human Reproduction Update
1026 2016;22:725–43. https://doi.org/10.1093/humupd/dmw028.
1027 [99] Duran HE, Simsek-Duran F, Oehninger SC, Jones HW, Castora FJ. The association of reproductive
1028 senescence with mitochondrial quantity, function, and DNA integrity in human oocytes at
1029 different stages of maturation. Fertility and Sterility 2011;96:384–8.
1030 https://doi.org/10.1016/j.fertnstert.2011.05.056.
1031 [100] May-Panloup P, Brochard V, Hamel JF, Desquiret-Dumas V, Chupin S, Reynier P, et al. Maternal
1032 ageing impairs mitochondrial DNA kinetics during early embryogenesis in mice. Human
1033 Reproduction 2019;34:1313–24. https://doi.org/10.1093/humrep/dez054.

bioRxiv preprint doi: https://doi.org/10.1101/2021.04.07.438786; this version posted April 9, 2021. The copyright holder for this preprint (which was not certified by peer review) is the author/funder, who has granted bioRxiv a license to display the preprint in perpetuity. It is made available under aCC-BY-NC-ND 4.0 International license.

[101] Rambags BPB, van Boxtel DCJ, Tharasanit T, Lenstra JA, Colenbrander B, Stout TAE. Advancing maternal age predisposes to mitochondrial damage and loss during maturation of equine oocytes in vitro. Theriogenology 2014;81:959–65. https://doi.org/10.1016/j.theriogenology.2014.01.020.

[102] Hendriks WK, Colleoni S, Galli C, Paris DBBP, Colenbrander B, Stout TAE. Mitochondrial DNA replication is initiated at blastocyst formation in equine embryos. Reprod Fertil Dev 2019;31:570. https://doi.org/10.1071/RD17387.

[103] Silva E, Greene AF, Strauss K, Herrick JR, Schoolcraft WB, Krisher RL. Antioxidant supplementation during in vitro culture improves mitochondrial function and development of embryos from aged female mice. Reprod Fertil Dev 2015;27:975. https://doi.org/10.1071/RD14474.

[104] Waelchli RO, MacPhee DJ, Kidder GM, Betteridge KJ. Evidence for the Presence of Sodium- and Potassium-Dependent Adenosine Triphosphatase alpha 1 and beta 1 Subunit Isoforms and Their Probable Role in Blastocyst Expansion in the Preattachment Horse Conceptus. Biology of Reproduction 1997;57:630–40.

[105] Nascimento AD do, Marques JCC, Cezar ARR, Batista AM, Kastelic JP, Câmara DR. Inhibition of Na+, K+ -ATPase with ouabain is detrimental to equine blastocysts. Anim Reprod 2020;17:e20190079. https://doi.org/10.21451/1984-3143-AR2019-0079.

Figures

Figure 1: Bisection of equine embryos at 8 days post-ovulation into an ICMandTE and a TE_part.

A) Step 1: Identification of the ICM and the TE; B) Step 2: Definition of the cutting plane to isolate the ICM in one of the parts; C) Step 3: Cutting of the embryo and separation of the two parts. ICMandTE: inner cell mass + trophoblast; TE part: pure trophoblast.

bioRxiv preprint doi: https://doi.org/10.1101/2021.04.07.438786; this version posted April 9, 2021. The copyright holder for this preprint (which was not certified by peer review) is the author/funder, who has granted bioRxiv a license to display the preprint in perpetuity. It is made available under aCC-BY-NC-ND 4.0 International license.

1058 NB: Here the trophoblast represents trophectoderm + endoderm and ICM is composed of epiblast
1059 cells.

1060

1061 Figure 2: Total RNA yield per embryo in relation to embryo diameter

1062 Green circles represent embryos from young mares (YM) and yellow squares represent embryos from
1063 old mares (OM). The used relation is exponential.

1064

1065 Figure 3: Gene expression in ICM and TE before and after deconvolution using DeMixT

1066 A) Venn diagrams of the differential gene expression in ICMandTE *vs* TE part (before deconvolution),
1067 DeMixT_ICM_cells *vs* DeMixT_TE_cells (after deconvolution) and DeMixT_ICM_cells *vs* TE_part (gene
1068 expression of ICM after deconvolution *vs* gene expression in TE_part without deconvolution); B)
1069 Principal Component Analysis of gene expression of DeMixT_ICM_cells, DeMixT_TE_cells, ICMandTE
1070 and TE part datasets.

1071 Deconvolution was used to isolate gene expression of ICM and TE cells in ICMandTE hemi-embryos.
1072 ICMandTE: inner cell mass + trophoblast; TE part: pure trophoblast. Here trophoblast represents
1073 trophectoderm + endoderm.

1074

1075 Figure 4: Analysis of differentially expressed genes (DEG) in embryos according to maternal age

1076 A) representation of down (blue) and upregulated (red) DEG in ICM (from DeMixT_ICM_cells data
1077 obtained after deconvolution of ICMandTE using DeMixT R package [33,34]) and TE (from TE_part
1078 dataset) of embryos from OM *vs* YM. Functional classifications (for down regulated genes in ICM and
1079 TE and for up-regulated genes in ICM) using GO Biological Process obtained with PANTHER online
1080 software are presented as pie charts. For upregulated DEG in TE, no functional classification was made.

bioRxiv preprint doi: https://doi.org/10.1101/2021.04.07.438786; this version posted April 9, 2021. The copyright holder for this preprint (which was not certified by peer review) is the author/funder, who has granted bioRxiv a license to display the preprint in perpetuity. It is made available under aCC-BY-NC-ND 4.0 International license.

1081 B) Bar chart presenting p-adjusted of most specific subclass pathways provided by PANTHER online
1082 software after statistical overrepresentation test (Fisher's Exact test and Benjamini-Hochberg
1083 correction) with the Human GO Biological Process annotation on down-regulated DEGs in ICM.

1084 DEG: Differentially Expressed Genes (FDR < 0.05); TE: Trophoblast; ICM: Inner Cell Mass; OM: Old
1085 multiparous mares; YM: young multiparous mares

1086

1087 Figure 5: GSEA clustering of the most perturbed terms in ICM and TE according to mares' age

1088 Nodes represent altered gene sets in ICM and TE (FDR < 0.05). Node size represents the gene set size.
1089 Node shape represents the gene set database: GO BP (circle) or KEGG (diamond). Blue nodes represent
1090 enriched gene sets in YM (NES < 0) while red nodes represent enriched gene sets in OM (NES > 0).
1091 Edges represent the level of connection between representative gene sets. This graph was performed
1092 using SUMER R package [44] and modified using cytoscape 3.8.2 [45]

1093 ICM: Inner Cell Mass; TE: trophoblast; FDR: False Discovery Rate; GO BP: Gene Ontology Biological
1094 Process; Kyoto Encyclopedia of Genes and Genomes; NES: Normalized Enrichment Score; YM: Young
1095 mares; OM: Old mares

1096

1097 Figure 6: Schematic representation of the observed effects of maternal aging on ICM and TE in equine
1098 blastocysts

1099 Normal blastocyst development from day 7 to day 9 is represented inside black square using literature
1100 [56,57]. Light blue boxes represent biological processes that are enriched in YM embryos and light red
1101 boxes represent biological processes that are enriched in OM embryos.

1102

1103 Additional file 1:

bioRxiv preprint doi: https://doi.org/10.1101/2021.04.07.438786; this version posted April 9, 2021. The copyright holder for this preprint (which was not certified by peer review) is the author/funder, who has granted bioRxiv a license to display the preprint in perpetuity. It is made available under aCC-BY-NC-ND 4.0 International license.

Additional file 1.png

Pipeline of biostatistical analysis

Once extracted, total RNA qualification and quantification were obtained using a Bioanalyzer. For sequencing, 5 ng/sample of total RNA were used for paired end RNA sequencing (I2BC platform) using Illumina NextSeq 500 high technology. Sequences were trimmed using Cutadapt. To determine XIST sequence, a *de novo* assembly was made using a mapping with STAR and StringTie. The GTF observed was aligned in IGV and XIST sequence was found at the known position (according to Pablo Ross personal communication). XIST sequence was included in EquCab 3.0 and a new mapping was performed using STAR. Counting was performed using featureCounts. The differential analysis was performed including embryo sex and diameter using Deseq2. A functional enrichment analysis of DEGs was performed using PANTHER web software. In another time, counts of all genes were normalized using Deseq2 and a gene set analysis (GSEA) was performed using the Gene Ontology (GO) biological process (BP) and the Kyoto Encyclopedia of Genes and Genomes (KEGG) databases with GSEA software form the Broad Institute. To reduce redundancy between terms, SUMER analysis was performed on enriched gene sets.

Additional file 2:

Additional file 2.pdf

Analysis of ICM enriched and TE part before gene expression deconvolution using DeMixT

On first page, the analysis of differential expressed genes is represented. The second page represent the results of the gene set enrichment analysis of ICMandTE gene expression. The third page presents the clustering of gene sets altered by maternal age from SUMER analysis of the GO BP and KEGG terms of mixed ICMandTE and TE_part.

bioRxiv preprint doi: https://doi.org/10.1101/2021.04.07.438786; this version posted April 9, 2021. The copyright holder for this preprint (which was not certified by peer review) is the author/funder, who has granted bioRxiv a license to display the preprint in perpetuity. It is made available under aCC-BY-NC-ND 4.0 International license.

1128 Additional file 3:

1129 Additional file 3.csv

1130 Differential gene analysis using DeSeq2 in ICMandTE of equine embryo at Day 8 post-ovulation

1131 Equine ensemble ID, orthologue human Ensembl ID, Orthologue human Entrez Gene ID, gene
1132 description, normalized counts for each sample of ICM and parameters obtained after Deseq2 analysis
1133 (log2FoldChange, pvalue and padj (after FDR correction)) of genes expressed in ICM enriched part
1134 (before gene expression deconvolution using DeMixT) of OM and YM embryos

1135 ICM: Inner cell mass; OM: old mares; YM: young mares

1136

1137 Additional file 4:

1138 Additional file 4.csv

1139 Gene set enrichment analysis results on gene expression comparing ICMandTE of embryos from old
1140 mares to young mares

1141 Gene Set Enrichment Analysis results (pathway name, GO accession when possible and size,
1142 Normalized Enrichment Score, p-value and FDR corrected q-value) for GO biological process and KEGG
1143 databases on ICMandTE gene expression table.

1144

1145

1146 Additional file 5:

1147 Additional file 5.csv

1148 Differential gene analysis using DeSeq2 in DeMixT_ICM_cells of equine embryo at Day 8 post-ovulation

bioRxiv preprint doi: https://doi.org/10.1101/2021.04.07.438786; this version posted April 9, 2021. The copyright holder for this preprint (which was not certified by peer review) is the author/funder, who has granted bioRxiv a license to display the preprint in perpetuity. It is made available under aCC-BY-NC-ND 4.0 International license.

Equine ensemble ID, orthologue human Ensembl ID, Orthologue human Entrez Gene ID, gene description, normalized counts for each sample of ICM and parameters obtained after Deseq2 analysis (log2FoldChange, pvalue and padj (after FDR correction)) of genes expressed in ICM (after gene expression deconvolution of ICMandTE using DeMixT) of OM and YM embryos

ICM: Inner cell mass; OM: old mares; YM: young mares

Additional file 6:

Additional file 6.csv

Differential gene analysis using DeSeq2 in TE_part of equine embryo at Day 8 post-ovulation

Equine ensemble ID, orthologue human Ensembl ID, Orthologue human Entrez Gene ID, gene description, normalized counts for each sample of ICM and parameters obtained after Deseq2 analysis (log2FoldChange, pvalue and padj (after FDR correction)) of genes expressed in TE of OM and YM embryos

TE: Trophoblast; OM: old mares; YM: young mares

Additional file 7:

Additional file 7.csv

Gene set enrichment analysis results on gene expression of DeMixT_ICM_cells of embryos from young and old mares

Gene Set Enrichment Analysis results (pathway name, GO accession when possible and size, Normalized Enrichment Score, p-value and FDR corrected q-value) for GO biological process and KEGG

bioRxiv preprint doi: https://doi.org/10.1101/2021.04.07.438786; this version posted April 9, 2021. The copyright holder for this preprint (which was not certified by peer review) is the author/funder, who has granted bioRxiv a license to display the preprint in perpetuity. It is made available under aCC-BY-NC-ND 4.0 International license.

1170 databases on DeMixT_ICM_cells gene expression table (after gene expression deconvolution on
1171 ICMandTE using DeMixT).

1172

1173 Additional file 8:

1174 Additional file 8.csv

1175 Gene set enrichment analysis results on gene expression of TE_part of embryos from young and old
1176 mares

1177 Gene Set Enrichment Analysis results (pathway name, GO accession when possible and size,
1178 Normalized Enrichment Score, p-value and FDR corrected q-value) for GO biological process and KEGG
1179 databases on TE_part gene expression table.

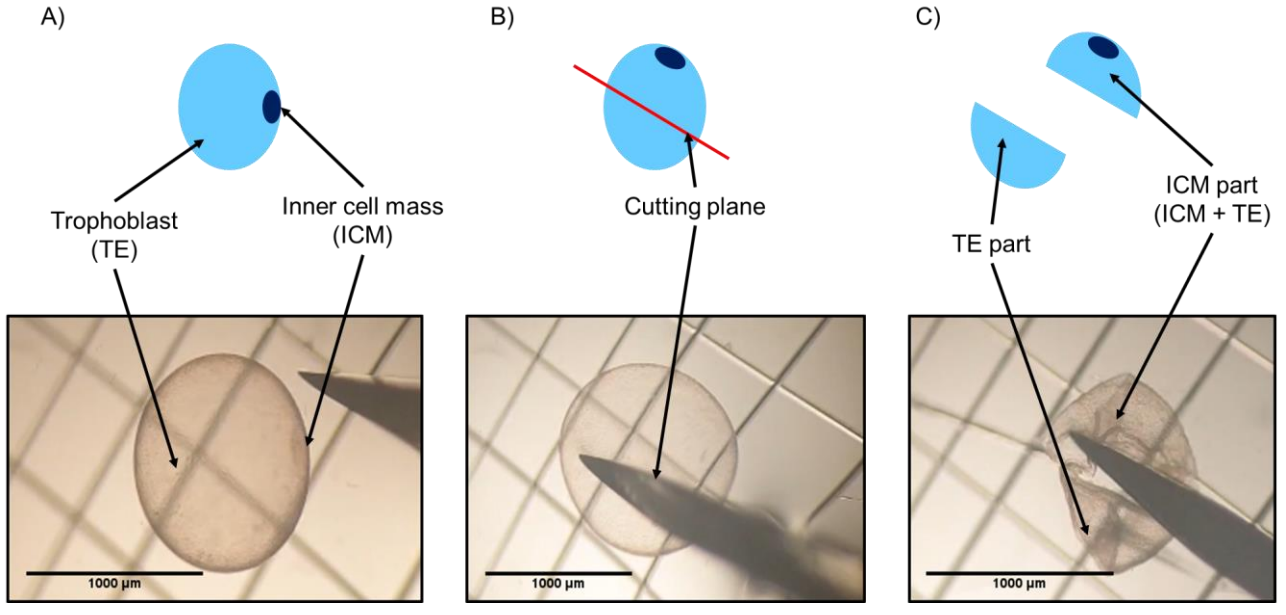
A)
Trophoblast
(TE)
Inner cell mass
(ICM)
1000 µm
B)
Cutting plane
1000 µm
C)
TE part
ICM part
(ICM + TE)
1000 µm

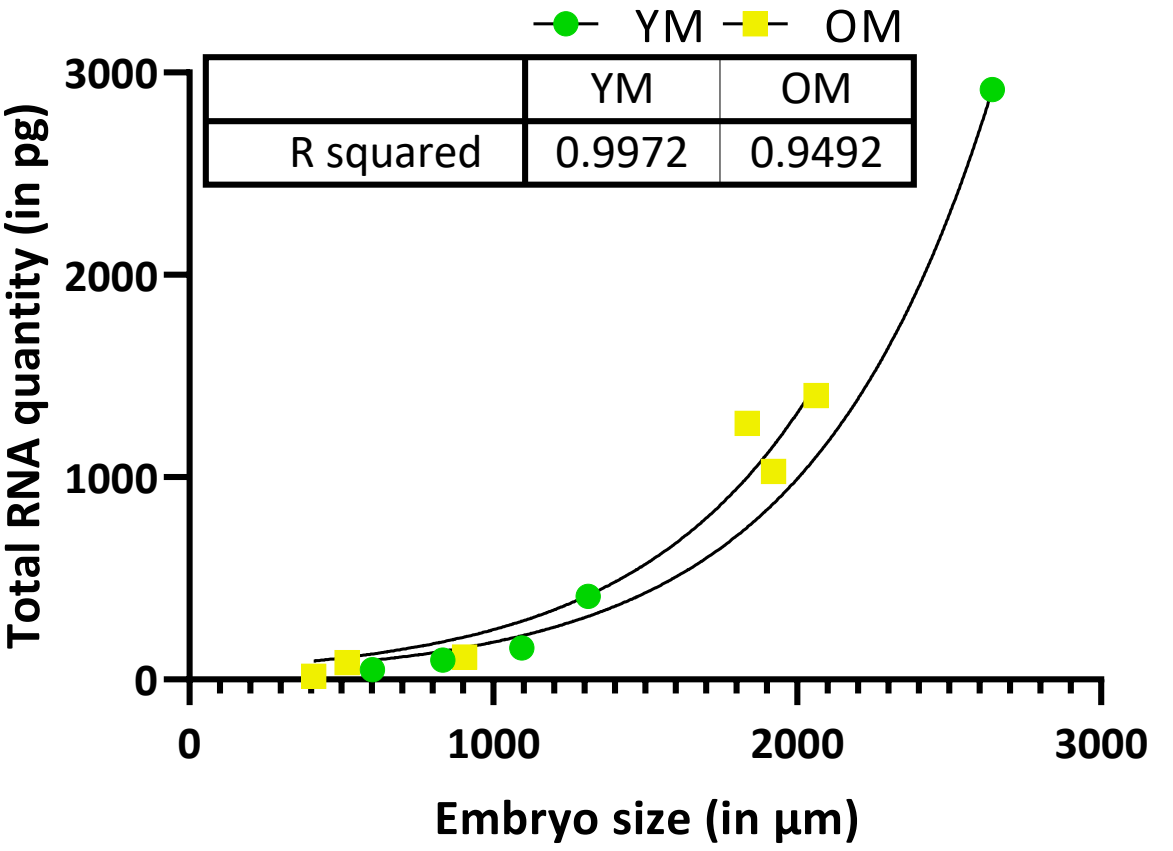
YM
OM
YM
OM
R squared
0.9972
0.9492
3000
2000
1000
0
Total RNA quantity (in pg)
0
1000
2000
3000
Embryo size (in µm)

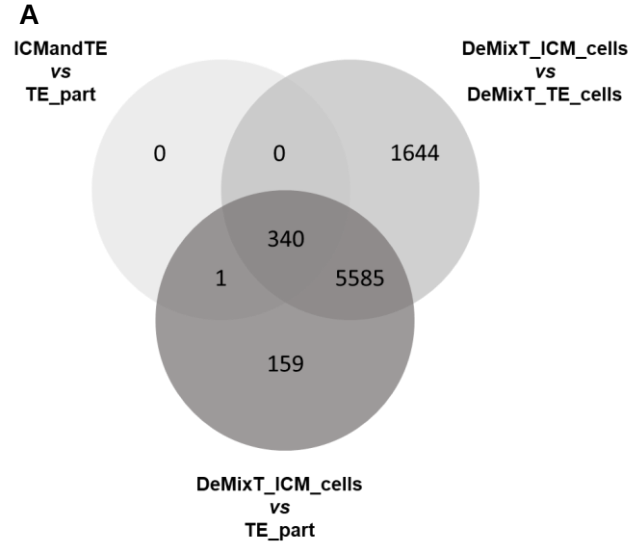
A
ICMandTE
vs
TE_part
DeMixT_ICM_cells
vs
DeMixT_TE_cells
0
0
1644
340
1
5585
159
DeMixT_ICM_cells
vs
TE_part

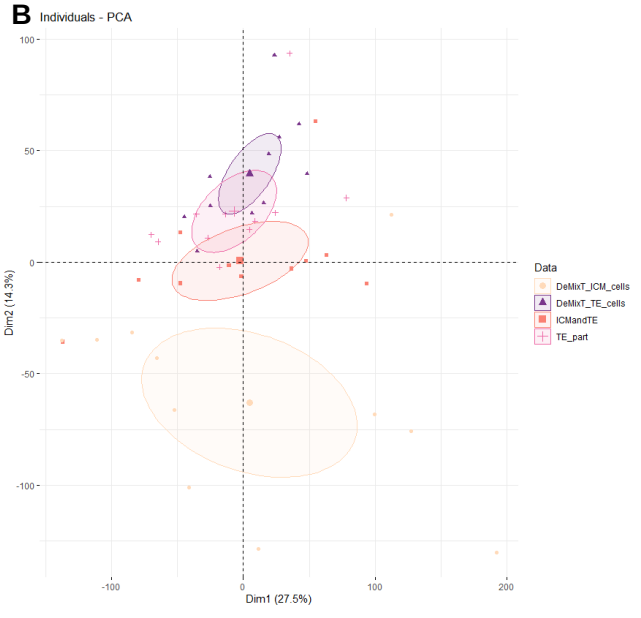
B
Individuals - PCA
100
50
0
-50
-100
Dim2 (14.3%)
-100
0
100
200
Dim1 (27.5%)
Data
DeMixT_ICM_cells
DeMixT_TE_cells
ICMandTE
TE_part

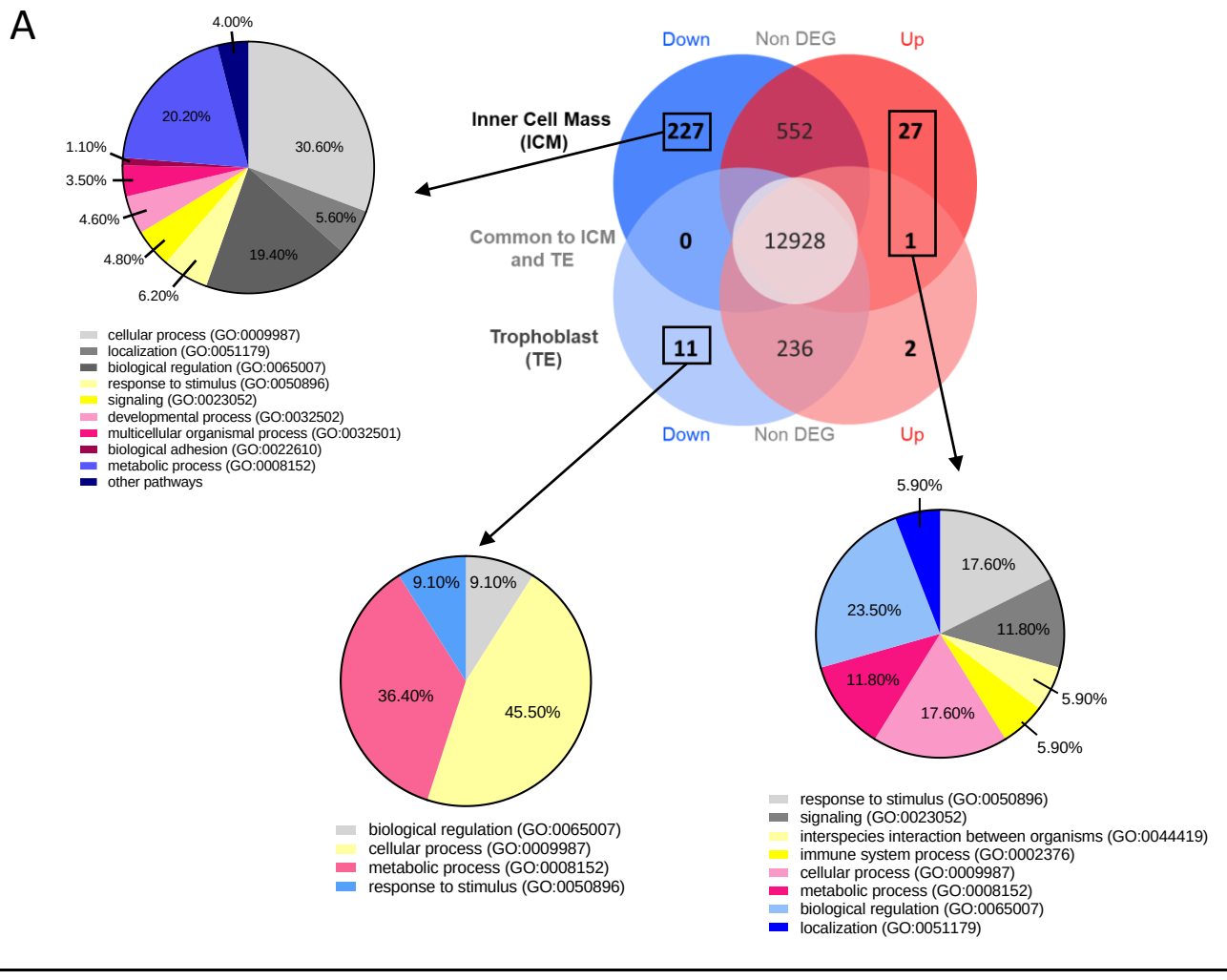
A
4.00%
20.20%
30.60%
1.10%
3.50%
5.60%
4.60%
4.80%
19.40%
6.20%
cellular process (GO:0009987)
localization (GO:0051179)
biological regulation (GO:0065007)
response to stimulus (GO:0050896)
signaling (GO:0023052)
developmental process (GO:0032502)
multicellular organismal process (GO:0032501)
biological adhesion (GO:0022610)
metabolic process (GO:0008152)
other pathways
Down
Non DEG
Up
Inner Cell Mass (ICM)
227
552
27
Common to ICM and TE
0
12928
1
Trophoblast (TE)
11
236
2
Down
Non DEG
Up
9.10%
9.10%
36.40%
45.50%
biological regulation (GO:0065007)
cellular process (GO:0009987)
metabolic process (GO:0008152)
response to stimulus (GO:0050896)
5.90%
17.60%
23.50%
11.80%
11.80%
5.90%
17.60%
5.90%
response to stimulus (GO:0050896)
signaling (GO:0023052)
interspecies interaction between organisms (GO:0044419)
immune system process (GO:0002376)
cellular process (GO:0009987)
metabolic process (GO:0008152)
biological regulation (GO:0065007)
localization (GO:0051179)

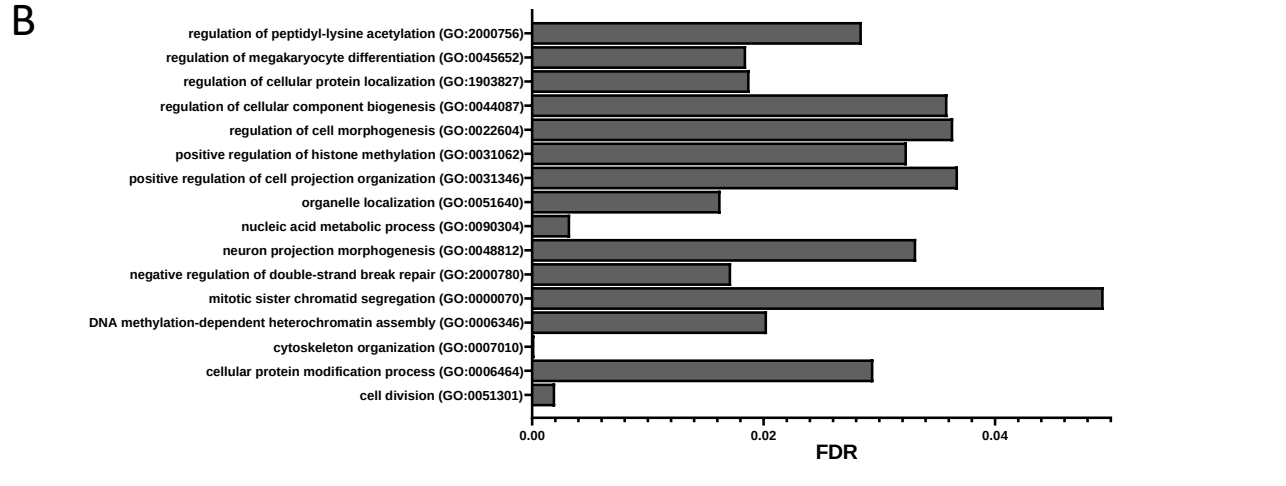
B
regulation of peptidyl-lysine acetylation (GO:2000756)
regulation of megakaryocyte differentiation (GO:0045652)
regulation of cellular protein localization (GO:1903827)
regulation of cellular component biogenesis (GO:0044087)
regulation of cell morphogenesis (GO:0022604)
positive regulation of histone methylation (GO:0031062)
positive regulation of cell projection organization (GO:0031346)
organelle localization (GO:0051640)
nucleic acid metabolic process (GO:0090304)
neuron projection morphogenesis (GO:0048812)
negative regulation of double-strand break repair (GO:2000780)
mitotic sister chromatid segregation (GO:0000070)
DNA methylation-dependent heterochromatin assembly (GO:0006346)
cytoskeleton organization (GO:0007010)
cellular protein modification process (GO:0006464)
cell division (GO:0051301)
0.00
0.02
0.04
FDR

Inner Cell Mass

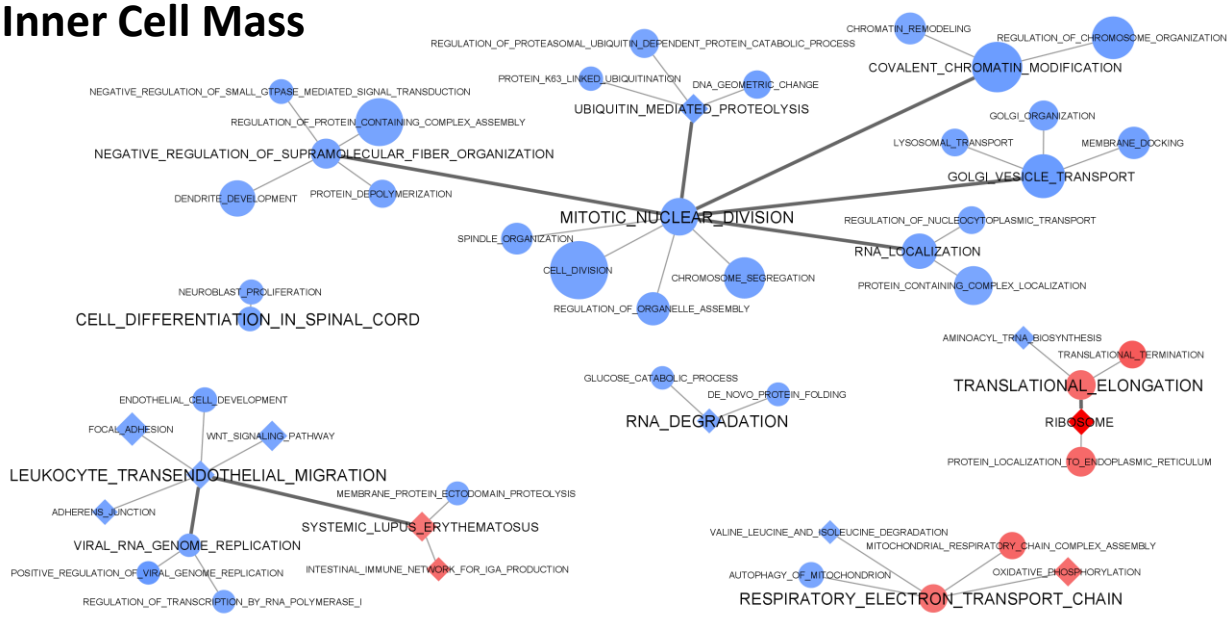

Trophoblast

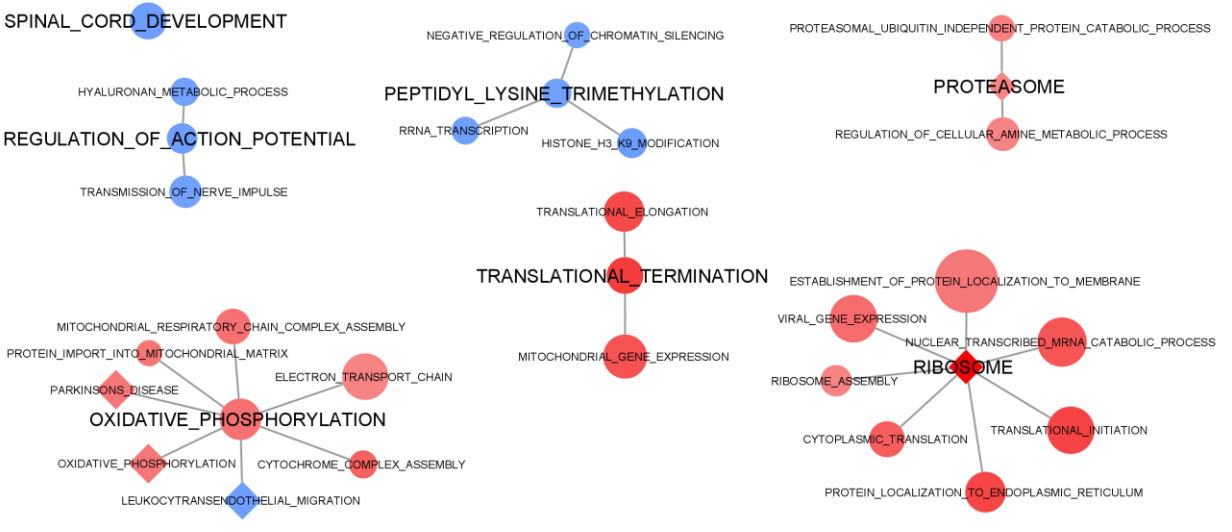

MATERNAL AGING

Cell cycle / Mitotic division
- → Assembly of spindle
- → Chromosome segregation
- → Cytokinesis/vesicle trafficking
- → Catabolism of protein and mRNA

Transcription
→ Chromatin modification

Cell signaling & adhesion
- → Wnt signaling pathway
- → Focal adhesion
- → Adherens junction

Embryo development
→ Cell fate commitment

Translation
→ Ribosome biogenesis

Mitochondrial function

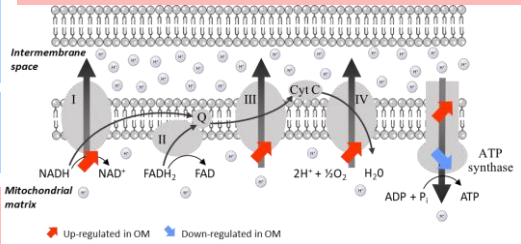

ALTERED ICM DEVELOPMENT

Normal **ICM** development

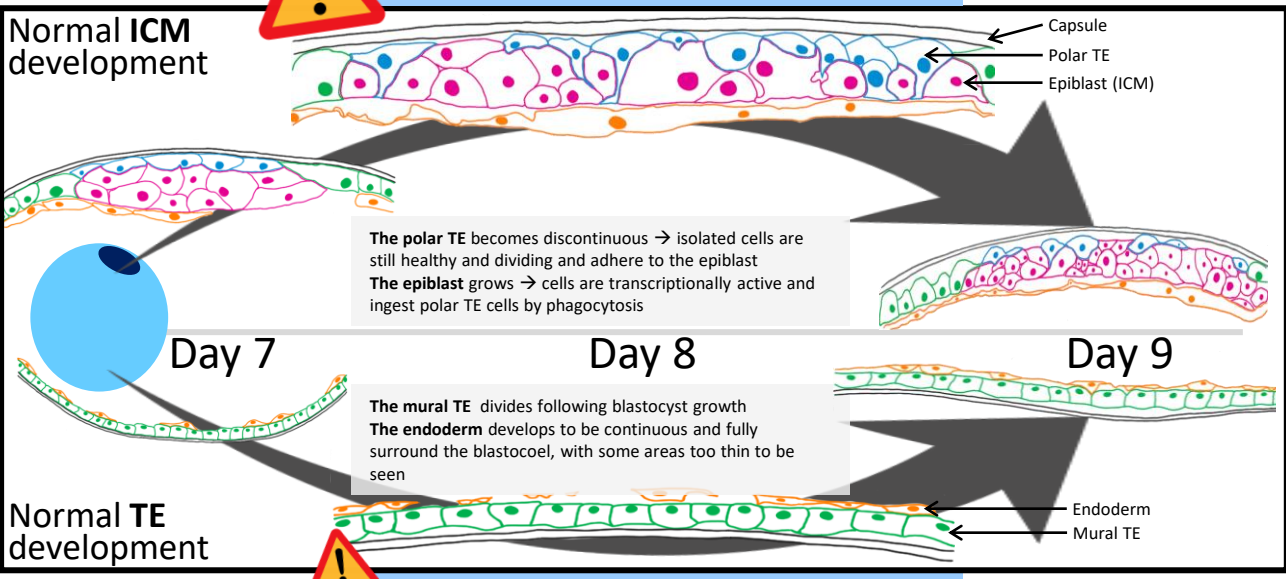

The polar TE becomes discontinuous → isolated cells are still healthy and dividing and adhere to the epiblast
The epiblast grows → cells are transcriptionally active and ingest polar TE cells by phagocytosis

The mural TE divides following blastocyst growth
The endoderm develops to be continuous and fully surround the blastocoel, with some areas too thin to be seen

Normal **TE** development

ALTERED TE DEVELOPMENT

Ion movement
→ Transmission of action potential

Transcription
→ Chromatin modification

Embryo development

Protein catabolism
→ Proteasome

Mitochondrial function

Translation
→ Ribosome biogenesis

MATERNAL AGING